Hydrostatic Analysis of a Suction-Stabilized Float

Luis Vendrell,
College of Technology & Innovation,
Arizona State University, Mesa, Arizona 85212, USA
E-mail:lvendrell@asu.edu

C.S Susheelkumar,
College of Technology & Innovation,
Arizona State University, Mesa, Arizona 85212, USA
E-mail: scherang@asu.edu

Sangram Redkar[1],
College of Technology & Innovation,
Arizona State University, Mesa, Arizona 85212, USA
E-mail: Sangram.Redkar@asu.edu

James W. Montgomery Jr. 2,
J. Montgomery Group L.L.C,
Scottsdale, Arizona 85258, USA
E-mail: jwmjraia@aol.com

ABSTRACT

This research examines the hydrostatic properties of a floating platform that uses a stability method known as Suction-Stabilization. This method differs from conventional methods of stabilization in that it utilizes an internal water chamber to raise the effective metacentric height through an inverse free surface effect. The specific case used in this report is a Suction-Stabilized Float meant for use in a backyard pool application. However, the analyses described can also be used for offshore floating structure applications, such as in a deep-sea wind turbine application. The study shows that Suction-Stabilization increases the stability of the float in both static and dynamic situations.

KEYWORDS

Metacentric height, Inverse slack tank effect, Righting moment, Righting lever

[1] Corresponding Author, Associate Professor, Arizona State University, Mesa, Arizona 85212, USA

2 Corresponding Author, Architect, Inventor, Discoverer of SSF Technology, Scottsdale, Arizona 85258, USA

INTRODUCTION

Offshore wind power is an untapped resource for renewable energy, which is available between 5 and 50 miles off the coast of the USA [2]. The use of floating platforms with wind turbines has been proposed as a method of utilizing this wind energy. Offshore wind platforms must be durable, able to support the weight of the wind turbine and be able to withstand both wind and wave loads and the roll and pitch motions associated with them [3]. These factors make stability a major concern when a floating platform is used in an offshore application.

It is conventional for a floating platform to gain its buoyancy force by the direct displacement of water [4]. Yet, there are other methods of stabilization and, in general, offshore platforms fall into one, or a combination, of three floating platform classifications: ballast, buoyancy, and mooring lines. All three of these classifications, when designed correctly, achieve a stable platform. However, all have drawbacks that must be weighed against their positives [3].

The most common of the above stated methods of stabilization is the use of mooring lines, or a Tension Leg Platform (TLP). However, the richest winds resources are located in ocean areas where the depth is greater than 30m. This presents a problem when a floating platform is located in deep sea regions where the depth is great, because the cost of TLP increases with depth. Mooring lines are not economically feasible in deep water [3]. Also, TLP's are complex and require significant onsite installation, unless significant design work is done to ensure it is stable in shallow draught water, and that it has a self-deploying anchoring mechanism to allow for deployment from port [3].

The *Ballast Classification* includes floating platforms that uses ballast weight or a ballast tank to increase stability. An example is a spar-buoy, which has a large ballast weight suspended beneath the floating platform to resist roll motion. While this classification has increased wave resistance, does not have the same cost problems associated with a TLP, and requires little onsite installation and maintenance, it does have some drawbacks. The suspended ballast requires a certain depth for

operation this renders float-out from port unfeasible unless, like the TLP, design work is done to ensure self-deployment of the suspended ballast weight once a proper depth is achieved. Also, the ballast tank/weight is complex and costly [3].

The *Buoyancy Classification* includes floating platforms that use a weighted water plane area to increase stability. An example of such a platform is a barge [3]. This allows for operation in all depths and allows for float-out from port. The simple shape of the barge allows for easier fabrication and it is less costly than both the TLP and spar-buoy. Its depth independence allows it to float freely without a specific location and to keep it in a central location requires the use of catenary mooring and anchor lines [3] .

In addition to these classifications, there are additional "add-on techniques" that increase the stability a floating platform of any of the above classifications. These techniques include adding a bilge keel, adding a roll fin, integrating a passive roll tank, or using a pneumatic roll tank. However, not all of these are economically feasible and not all of them are compatible with the use of a wind turbine. The requirements for such an application are a floating platform that is stable, is compatible with a wind turbine and is economically feasible.

A Suction-Stabilized floating platform, or Suction-Stabilized Float (SSF), is one alternate option that was found to be well suited for offshore wind applications. It is a combination of the ballast and buoyancy classifications. An SSF is designed with an internal void to trap water above the water plane. This trapped water acts as a ballast with a moving center of gravity that acts further from the center of floatation with increased roll angle. This ballast will increase the restoring force of the float and aide in the resistance of roll and pitch [6, 8].

This study presents a mathematical model for a suction stabilized float platform with the goal of defining the hydrostatic properties, determining the stability criteria, narrowing down the factors that increase or decrease stability, and suggesting methods to increase stability.

BACKGROUND

The method of analyzing the stability of a ship has been fully described by A B Biran in his book [1]. The most important metrics with respect to ship stability are the metacentric height ($\overline{GM}$) and the righting lever ($\overline{GZ}$). The metacenter is the intersection of the line of action of the buoyancy force when the ship is upright and the line of action of the buoyancy force when the ship heels to an angle, ϕ [1]. Stability is maintained as long as the metacenter is vertically above the center of gravity of the ship. For large angle of heel, greater than 7°, metacentric height is not an accurate measure of stability. Beyond this angle, inclined waterlines no longer intersect the centerline and the metacenter moves away from its previous position [7]. Because of this, for heel and pitch angle above 7°, another metric must be used to determine stability.

The righting moment, as defined by Euler, is an alternate metric used to determine ship stability when the heel angle is large. This metric relates the couple of the gravitational force and the buoyancy force of the ship to ship stability. As long as the couple of these two forces causes a restoring or righting moment, which returns the ship to equilibrium, the ship remains stable [5].

Reference [1] defines the righting moment as the product of the distance between the center of buoyancy and the ship center of gravity and the weight of the ship.

$$M_R = W_{ship} * \overline{GZ} \quad \textbf{(1)}$$

Where M_R is the righting moment, W_{ship} is the weight of the ship, and $\overline{GZ}$ is the horizontal distance between the ship center of gravity and the ship center of buoyancy [1].

The value $\overline{GZ}$ characterizes the righting moment.

$$\overline{GZ} = \ell_k - \overline{KG}\sin\phi \quad \textbf{(2)}$$

Where ℓ_k is the value of stability cross-curves and is usually determined with the use of a computer, and $\overline{KG}$ is the vertical distance between the bottoms-most point on the ship and the ship center of gravity. The relationship between value of stability cross-curves, ℓ_k, and the heel angle, ϕ, is not linear and, in general, cannot be defined explicitly. However for small angles, the value of the righting lever can calculated using the metacentric height [1].

$$\overline{GZ} = \overline{GM} \sin \phi \quad \textbf{(3)}$$

Eq. (3) is only valid for small angles, and the definition of a small angle is dependent on the specific ship [1]. In general, a small angle is one where the metacenter does not move visibly from its initial position in equilibrium.

The methods used in this text [1] are the basis for the static analyses in this study. The equations defined in this text are for a ship and not a floating platform. The methods used in this text, while applicable, must be altered to account the geometry of the float. In general, a float is a much simpler geometry than a ship. A ship is, usually, symmetric around one axis, whereas a float is symmetric around two.

Reference [6] describes the embodiment for a Suction-Stabilized Float (SSF). The SSF is a float that has a buoyant portion and a chamber portion that holds liquid within an internal volume above the interface, or waterline, of the surrounding fluid [6]. The fluid trapped above the waterline creates a downward force that adds to the restoring moment of the SSF. It acts in the same way as an anti-roll tank, only the volume is open to the submerging fluid rather than the atmosphere [6]. The SSF used for this report is one of the many embodiments described in the patent application.

SUCTION STABILIZED FLOAT

A suction-stabilized float (SSF) is a float platform that can, but does not require the use of devices such as mooring lines, bilge keels, and passive roll tanks to increase stability. Instead, the SSF

utilizes an internal volume that is closed to the atmosphere and opens to the fluid in which it floats [6,8].

Figure 1 shows an example of SSF geometry. In general, it is a float platform with more than one diameter consisting of a smaller diameter lower section and a larger diameter upper section. The internal volume is hollow so that fluid can fill it completely. The SSF is sealed to the atmosphere and open to fluid. The geometry of the SSF is such that the waterline lies within the lower and upper limits of the larger volume. The effect of this is to trap the fluid above the water line. The trapped water is in contact with the walls of the SSF on all sides except the bottom, where it is open to the fluid.

The body construction uses a material with a density much lower than that of the fluid in which it is submerged. This allows the fluid trapped inside the SSF to act as ballast. However, the effect of the trapped water does more than simply act as ballast. It also adds to the overall stability of the SSF by raising the effective metacentric height [6,8].

When a floating platform or ship has an in internal volume that is not enclosed on all four sides it is called a *slack-tank*. The effect of this *slack-tank* is to lower the metacentric height through a phenomena known as the “free surface effect” [1]. However, in the case of the SSF, the internal tank does not open to air but rather opens to the submerging fluid. The result of this is that the internal volume acts as an Inverse Slack Tank (IST) and raises the metacentric height rather than lowering it [8].

In the case of a slack tank, when the ship or platform rotates away from equilibrium to any heel angle, the surface remains horizontal while the fluid in the tank conforms to the angle of heel. This results in an added wedge of fluid in the direction of heel and a subtracted wedge of fluid, of the same volume, on the side opposite of heel. This acts as a moving mass from one side of the ship or platform in the direction of heel and increases the heeling moment, which decreases stability.

For the SSF, the IST acts in an opposite manner. The ballast fluid trapped inside the internal volume shifts when the float undergoes either a roll or a pitch motion. When the SSF is subjected to a

roll or pitch motion, the shape of trapped water along the waterline changes. For example, in the case of a small heel angle, when the SSF heels towards portside (left-side), in a stable waterline the volume on the left side of the SSF is reduced, while the volume of starboard (right-side) is increased. For small heel angles, these volumes are equivalent and the mass of the trapped fluid does not change. Therefore, the volume that is subtracted from the port side is added to the starboard side. This results in a shift of the center of gravity of the trapped fluid towards starboard. The net result is an additional righting moment that brings the SSF back to its equilibrium position, which is the opposite of free surface effect. For larger angles of heel, however, the mass of the trapped water increases to account for volumetric changes and increases the IST effect of the trapped water and increases the righting moment.

The SSF can be used as a platform to hold a mast, either an umbrella or a wind turbine. Problems arise from the high center of gravity of the mast when attached to the SSF. Without the ballast mass of the "inverse slack tank," the center of gravity falls above, or close to, the metacenter and the float becomes unstable. The IST acts to both raise this metacenter and increase stability [8].

For the SSF to function as it is intended it is necessary for the SSF to act as a closed system with the atmosphere, and that no air enters the internal volume. Once the internal volume is open to the atmosphere and air is allowed to enter water no longer fills the entire internal volume of the SSF. This negates the IST effect and causes the trapped water to act a standard slack tank and lowers the effective metacentric height rather than increases it.

This extreme value of roll or pitch is defined as the *Air Entrance Angle,* α . This is not to be confused with the *Angle of Vanishing Stability,* ϕ_{VS} , which is the angle at which the righting moment becomes negative. However, both of these angles are significant in that they signify when the SSF is no longer stable. As a general statement of stability, *the SSF becomes unstable at the lesser of the two angles* ϕ_{VS} *and* α .

This study analyzes a specific case of a SSF detailing the methodology with calculations for studying stability. The stability of this SSF is analyzed in both static and dynamic situations. In this

paper, the hydrostatic analysis is presented in detail with an example. The hydrodynamic studies of SSF will be presented in another paper. The platform analyzed is this work is a scaled model of one intended for use in a deep-sea wind turbine application. The intention and purpose of this reduced scale platform is to serve as the floating base for an umbrella used in a backyard pool. However, the dynamics and analysis of this model are applicable to that of a larger model and can be adapted to an SSF used in a wind turbine application.

The SSF is a circular float with an empty internal volume. The baseline geometry is shown in Figure 3. The body of the SSF is made of a polyurethane foam, the material of the top plate is an acrylic/Plexiglas circular plate, and the fluid is salt water.

Table 1 lists the given densities used for the analyses for the study. All masses are calculated using the values in Table 1. Figure 4 defines the cross-section for the baseline SSF geometry. This geometry is the initial geometry used for analysis. Special cases are analyzed and compared to this baseline in the following sections when a comparison is necessary. Unless specified, any analysis in this paper refers to the baseline geometry.

Table 2 lists all pertinent properties of the baseline geometry. When the variation of the baseline geometry is analyzed, the properties listed in Table 2 are not explicitly shown, but are calculated using the same methods. Table 3 lists all masses needed to calculate the hydrostatic properties of the baseline SSF in calm water at 0° heel.

Coordinate System

It is important to note the coordinate system used, as shown in Figure 5. The standard ship coordinate system and nomenclature, as defined by A B Biran, is used for this study [1].

- Translation in the X-Direction is referred to as Surge.
- Translation in the Y-Direction is referred to as Sway.
- Translation in the Z-Direction is referred to as Heave.
- Rotation about the X-Axis is referred to as Roll.

- Rotation about the Y-Axis is referred to as Pitch.
- Rotation about the Z- Axis is referred to as Yaw.

It is apparent from Figure 5 that the baseline SSF is symmetric around both the **xOz** axis and the **yOz** axis and that these cross-sections are identical to one another. This results in equivalent Surge and Sway translations and pitch and the roll rotations. In other way, when any incident force is applied at any location perpendicular to the Z-axis that incident direction can be defined as either the X-axis or the Y-axis.

HYDROSTATIC ANALYSIS: SSF WITHOUT MAST

This section presents the calculation method used in this report for determining the Hydrostatic properties of the baseline SSF without a mast attached. All calculations in this section are based on the analyses presented in [1].

Metacentric Height at 0° Heel.

Metacentric height, $\overline{GM}$, is calculated by the following equation [1],

$$\overline{GM} = \overline{BM} + \overline{KB} - \overline{KG} \quad \textbf{(4)}$$

Where, $\overline{BM}$ **,** is the metacentric radius, $\overline{KB}$, is the distance from the base point (K) to the center of buoyancy, and $\overline{KG}$ is the distance from the base point (K) to the center of gravity of the float.

Metacentric Radius.

Metacentric radius, $\overline{BM}$, is calculated by Eq. (5).

$$\overline{BM} = \frac{I_{wp}}{V_{dis}} \quad \textbf{(5)}$$

Where, I_{wp} is the Area Moment of Inertia of the water plane and V_{dis} is the total volume displaced. I_{wp} is found in Table 1**.**

$$I_{wp} = I_{bS4} + I_{wS4} = 39{,}762 in^4 \quad \textbf{(6)}$$

V_{dis} is calculated by using the value of draught, T, calculated by equating the mass of the water displaced due to immersion of the SSF

$$V_{dis} = (91.10 in^2)(5.26 in) + 622.10 in^3 = 1101.29 in^3$$

The water plane area moment of inertia used, since the waterline lies in Section 4, is that of Section 4, found in Table 2.

$$\overline{BM} = \frac{I_{wp}}{V_{dis}} = \frac{39{,}762 in^4}{1101.29 in^3} \quad \textbf{(7)}$$
$$\overline{BM} = 36.105 in$$

SSF Center of Gravity.

The center of gravity, $\overline{KG_t}$, is calculated by a mass balance of the float mass and the ballast water mass.

$$\overline{KG_t} = 5.98 in \quad \textbf{(8)}$$

Center of Buoyancy.

The center of buoyancy, $\overline{KB}$, is calculated by a mass balance of the SSF mass below the waterline.

$$\overline{KB} = 3.60 in \quad \textbf{(9)}$$

Metacentric Height without IST (or Suction Stabilization) Effect.

Metacentric Height is calculated using Eq. (4)

$$\overline{GM} = 36.11in + 3.60in - 5.98in$$
$$\overline{GM} = 33.73in \quad \textbf{(10)}$$

IST (or Suction Stabilization) Effect on Metacentric Height.

The water in this region acts like an inverted tank with the free surface open to the water beneath. With this in mind, the IST is treated in the opposite fashion as that of a free surface slack tank open to the atmosphere [8]. Whereas the free surface tank results in an effective metacentric height that is lower than the metacentric height of the body alone, the inverted tank will raise the metacentric height.

$$l_F = \frac{I_{w4}}{V_{dis}} \quad \textbf{(11)}$$

$$l_F = \frac{30{,}172in^4}{1101.29in^3} = 27.40in$$

$$\overline{GM}_{eff} = \overline{GM} + l_F \quad \textbf{(12)}$$

$$\overline{GM}_{eff} = 33.73in + 27.40in$$
$$\overline{GM}_{eff} = 61.13in$$

Comparison: Non-SSF and SSF

It is important to compare the baseline SSF to that of a float with the same geometry that does not utilize suction stabilization. This requires the internal volume of the float to operate as an open system with the outside atmosphere. When the internal volume is not a closed system there is no ballast water trapped above the waterline and the draught is dependent only on the mass of the float.

From

Table 4, it is observed that a float with Suction-Stabilization compared to a float without Suction-Stabilization has a higher effective metacentric height. Note that the draught is much lower and lies in Section 2, which will leave more than half of the float body above the waterline.

$$\Delta\overline{GM} = \overline{GM}_{SSFeff} - \overline{GM}_{NSSF} = 61.13in - 44.82in = 16.31in$$

Thus it is verified that Suction-Stabilization increases the $\overline{GM}_{eff}$ of the baseline geometry when compared to a float that does not utilize Suction-Stabilization.

PARAMETRIC STUDIES:

In this section, we study the effect of important float dimensions on the stability of the float.

a) Geometric Variation: Section 4 Height.

The height of Section 4 is important in that it can drastically change the allowed volume of trapped water ballast. It is important to examine this parameter and its effects on the hydrostatic properties of the SSF.

Figure 6 defines the initial and final heights used. Note the baseline height was used as the initial case. When the height of Section 4 is less than that of the baseline the waterline of the SSF no longer falls within the vertical limits of Section 4, which may lead to an unstable condition. The methods used to determine the metacentric height is the same as in Eq. (4) and Eq. (12)

Figure 7 plots the draught against the height of section 4. The draught increases linearly with the height of Section 4. Looking at the equations utilized for the draught calculation, we get

$$\sum_{1}^{i=5}\left(A_{bi}H_{bi}\right) + A_{wS4}\left(\sum_{1}^{i=5}H_{Si} - T\right)\rho_{SW} = \rho_{SW}\left[T - \left(\sum_{1}^{i=3}H_{Si}\right)\right]A_{bS4} + \left(\sum_{1}^{i=3}V_{bSi}\right) \quad \textbf{(13)}$$

$$\Rightarrow T = \frac{\left[\left(\frac{\sum_{1}^{i=5}\left(A_{bi}H_{bi}\right)}{\rho_{SW}}\right) + A_{wS4}\left(\sum_{1}^{i=5}H_{Si}\right) + \left(\sum_{1}^{i=3}H_{Si}\right)A_{bS4} - \left(\sum_{1}^{i=3}V_{bSi}\right)\right]}{\left(A_{wS4} + A_{bS4}\right)} \quad \textbf{(14)}$$

Where H_{bi} is the height of ith base section of SSF, H_{Si} is height of ith section, A_{si} is Area of SSF of ith section, V_{bSi} is volume of SSF base in each section

From Eq. (14), it is seen that as the Section 4 increases so does the draught. This is because the following quantities, $\left(\frac{\sum_{1}^{i=5} (A_{bi} H_{bi})}{\rho_{SW}} \right)$ and $A_{wS4} \left(\sum_{1}^{i=5} H_{Si} \right)$, are in the numerator and increase with the height of Section 4 while the remaining variables remain constant.

Using Eq. (14) in Eq. (8), the only term that changes value is T, and since T increases with the increase in Section 4 height, the displaced volume also increases. This results in a lower metacentric radius, and thus a lower metacentric height, because the Area Moment of Inertia of the water plane remains constant while the displaced volume increases.

Figure 9 plots the properties used to determine metacentric height against the height of Section 4. As predicted by Eq. (14), as the height of Section 4 increases, the effective metacentric height decreases.

Geometric Variation: Outer and Inner Diameters of Section 4.

The second geometric variation explored was increasing the outer diameter of the SSF and the inner diameter of Section 4 & 5 while keeping the outer and inner diameters of Section 1, 2, & 3 constant and how this affects the draught and metacentric height of the SSF.

Figure 11 plots the draught against the increasing outer and inner diameters of Section 4 & Section 5, as shown in Figure 10. As these diameters increase the draught decreases.

All terms, in both the numerator and denominator, on the right hand side of Eq. (14) increase with the increase of the outer and inner diameters of Section 4 & Section 5. From Figure 11, it is seen that the denominator increases at a faster rate than the numerator, which results in a decreased draught.

However, it is necessary to state that a decreased draught does not result in a decreased displacement volume. Figure 12 shows that the displacement volume increases as the outer diameter increases. Since the density of the SSF is significantly less than that of the water, a larger submerged volume does not equate to a large displacement mass.

From the equation for the volume of displacement, we get

$$V_{dis} = \left[\left(T - \left(\sum_{1}^{i=3} H_{Si}\right)\right) * A_{bS4}\right] + \left(\sum_{1}^{i=3} V_{bSi}\right) \quad \textbf{(15)}$$

In Eq. (15) A_{bS4} and $\sum_{1}^{i=3} V_{bSi}$ increase with the outer and inner diameters of Section 4 & Section 5, which is much greater than the decrease in T. This results in an increased displacement volume.

Figure 13 plots the properties used to determine metacentric height against the increasing outer diameter. As the outer diameter increases the effective metacentric height increases. The increase in metacentric height is a direct effect of the offset increase in the displaced volume with the much greater increase in both the SSF total water plane area moment of inertia and the ballast waters area moments of inertia.

Geometric Variation: Outer and Inner Diameters of All Sections.

The third geometric variation explored was increasing all diameters of the SSF by the same amount, as shown in Figure 14 and how this affects the draught and metacentric height of the SSF.

Figure 15 plots the draught against the increasing inner and outer diameters. As all diameters increase uniformly, the draught also increases.

All terms, in both the numerator and denominator, on the right hand side of Eq. (14) increase with the increase of the outer and inner diameters of Section 4 & Section 5. From Figure 15, it is seen that the denominator increases at a slower rate than the numerator, which results in an increase in draught.

Figure 16 plots the displaced volume against the increasing diameter. Comparing this to Figure 8, it is seen that while the displaced volume increases, but it does not increase as much as the geometry changes in Figure 12. This result stems from the fact that Section 3 of SSF, while it does see a volume increase, it does not have the same volume and mass increase as when the inner and outer diameters of Section 1 are held constant.

Figure 17 plots the properties used to determine metacentric height against the increasing inner and outer diameter. As both the inner and outer diameter increases, the effective metacentric height also increases. It is noted that, the increase in metacentric height is greater when all diameters of the SSF are increased in unison. This is due to the lower displacement volume and an increased area moment of inertia.

MAST SIZING AND OPTIMIZATION

The SSF is designed to specifically hold either an umbrella, in the case of backyard pool application, or, in the case of deep-sea application, a wind turbine. Both have relatively similar physical properties, a tall cylindrical shaft that rises vertically from the SSF and a mass mounted on the top of the shaft. It is fairly easy to infer that this will both increase the mass of the SSF and raise the Center of Gravity. Both metrics are important in determining stability. This section evaluates mast height and weight and how it affects the hydrostatic properties of the Baseline SSF. *Metacentric height* and *Kempf factor* are two metrics that will determine the ideal mast size.

Kempf Factor

The Kempf factor is a non-dimensional number used to evaluate the free roll characteristics of a ship or floating platform. It is used to determine where a ship or floating platform's motions are *tender, comfortable,* or *stiff*. Tender motions result from a large roll period and are associated with low metacentric heights. Comfortable motions signify that the roll period is balanced for the ship or floating body. Stiff motion results in short rolls periods that may become too violent (Biran 2003) .

The SSF is symmetric about both the X and Y-axes, it is assumed that roll and a pitch are equivalent and therefore the Kempf factor is applicable to both of these motions.

$$KEMPF = P_{roll}\sqrt{\frac{g}{D_O}} \tag{16}$$

Where g the gravitational constant is in $\frac{in}{s^2}$, D_O is the outer diameter of the float, and P_{roll} is the natural roll period of the float.

$$\omega_{roll} = \sqrt{\frac{g\overline{GM}}{i_m^2}} \tag{17}$$

$$P_{roll} = \frac{2\pi}{\omega_{roll}} \tag{18}$$

Where, ω_{roll} is the natural angular frequency of free roll of the SSF, i_m is the mass radius of gyration, and $\overline{GM}$ is the metacentric height as defined in Eq. (12). The value of the Kempf factor determines the float motions [1].

- For Kempf factor values **below 8**, the float motion is STIFF.
- For Kempf factor values **between 8 and 14**, the float motion is COMFORTABLE.
- For Kempf factor values **above 14**, the float motion is TENDER.

The purpose of using this metric is to determine the mast height and weight results in a roll period that would neither cause a motion that is too stiff nor too tender.

Mast Geometry Assumptions.

For the following analysis, a mast is defined as a vertical, thin cylindrical rod with a spherical mass at its highest point, as shown in Figure 18. This geometry simulates either an umbrella or a wind

turbine and will be used to determine the mast used for the remainder of this paper. The assumptions used to define mast geometry are listed below:

1. The mast body is a cylinder with a concentrated mass with its center at the highest point of the body cylinder. The mast attaches to the suction-stabilized platform at its center.
2. The concentrated mass is half of the mass of the body cylinder.
3. The mast has a uniform density.
4. The of gravity is found by the following equation,

$$KG_{mast} = \frac{2H_{mast}}{3} + H_{body} \quad \textbf{(19)}$$

Input Parameters for Mast Study

Using the initial geometry for the Baseline SSF, seven different mast heights were used to analyze the mast effect on the SSF.

Mast Size Limits

First, it is important to determine the mast weight at which the water line rises above the limits of Section 4. Figure 19 show the draught change based solely on the added weight of the mast. The black line illustrates the maximum draught allowable for the waterline to remain within the upper and lower bounds of Section 4. The red line illustrates the increasing draught as the mast weight increases. From Figure 19, it is seen that when the mast weight exceeds 36 lbs, the waterline falls above the limit of Section 4.

Next, it is imperative that the metacentric height remain positive. A negative metacentric height, in most cases, leads to instability [1]. To ensure a positive metacentric height, the weight of the mast is limited by the upper extreme value of 35lbs and the metacentric height is calculated for a range of mast weights between 0-35 lbs.

Figure 20 shows that metacentric height becomes negative for a mast height of 105 in at 35 lbs. To insure against a negative metacentric height, the mast weight is limited to an upper extreme of 33 lbs.

Mast Selection Criteria.

Each of the seven mast geometries shown in Table 5 were analyzed by iterating the mast weight from 0lbs to 33lbs. Figure 21 shows that for all mast heights, as the weight of the mast increases the metacenter decreases. The taller the mast, the higher its center of gravity and the more massive the mast, the more that center of gravity location plays a role in determining the metacentric height. Referring to Eq. (4), $\overline{GM} = \overline{BM} + \overline{KB} - \overline{KG}$, a higher $\overline{KG}$ will reduce the metacentric height as will the larger V_{dis} that is a result of the added weight of the mast. Stability decreases with both increasing mast height and increasing mast weight.

Figure 22 shows that, for all mast heights, as the weight of the mast increases the Kempf factor also increases. This results in a larger roll period for masts with higher centers of gravity and higher weight. A low mast center of gravity results in a *stiffer* float motion and a high center of gravity results in a *more tender* motion. It is desirable to use a mast that will result in a *comfortabl*e roll motion or a *moderately stiff* motion. Using these criteria, i.e. a Kempf factor between 8 and 14, and the mast heights between 15in and 105in a range for *comfortabl*e float motion is found.

Table 6 gives the appropriate mast weight for a certain mast height that will result in a *comfortable* float motion. It is also interesting to note the correlation between the Kempf factor and the metacentric height of the SSF.

Figure 23 plots the correlation between the Kempf factor and the metacentric height. The lower values of mast height have a smaller variation in metacentric height and therefore the Kempf factor does not vary as it does with taller masts. The Kempf factor increases as the metacentric height approaches zero. This implies that the lower the metacentric height the larger the roll period of the SSF.

Adding the mast to the SSF increases the center of gravity, displaced volume, center of buoyancy, and the draught. It decreases the metacentric radius, the metacentric height, the inverse free surface effect, and the effective metacentric height. The most important of these factors being the effective metacentric height, which is determined by the metacentric radius, the center of buoyancy, and the center of gravity. The taller and more massive the mast, the more adversely it will affect the metacentric height.

HYDROSTATIC ANALYSIS: SSF WITH MAST

This section presents the hydrostatic properties of the baseline SSF with a mast. The SSF is then compared to a float with the same basic geometry that does not utilize Suction-Stabilization. It then expands the analysis to the same geometries examined in Figure 6 and Figure 14.

SSF Properties with Mast.

The mast chosen was based on a nine-foot round patio umbrella. The hydrostatic properties were calculated using the methods shown in Eq. (12). The SSF weight and center of gravity was adjusted for the added mast weight, as shown in Figure 24, which lowers the metacentric height, the trapped water ballast volume and mass, and increases the draught, the SSF center of gravity, and the displaced volume.

Roll period and the Kempf factor are calculated using the values in Table 7

$$\omega_{roll} = 2\pi\sqrt{\frac{g\overline{GM}}{i_m^2}} = 2.908\,\frac{rad}{\sec} \tag{20}$$

$$P_{roll} = \frac{2\pi}{\omega_{roll}} = 2.16\sec \tag{21}$$

$$KEMPF = P_{roll}\sqrt{\frac{g}{D_O}} = 7.75 \tag{22}$$

Comparison: Non-SSF and SSF.

Table 8 shows that the inverse slack tank effect of the ballast water serves to increase the metacentric height significantly when compared to float platform that does not utilize Suction-Stabilization.

$$\Delta\overline{GM} = \overline{GM}_{SSFeff} - \overline{GM}_{NSSF} = 37.46in - 11.09in = 26.37in$$

Thus it is verified that Suction-Stabilization increases the $\overline{GM}_{eff}$ of the baseline geometry when compared to a float that does not utilize SS.

Geometry Variations.

The same geometries examined earlier, were examined again with the added weight of the mast and the resulting increase in center of gravity and draught.

Figure 25 plots the various properties of the SSF against an increasing Section 4 height. The trends seen with the mast included are the same as when there is no mast attached. However, the metacentric height and the effective metacentric height are much lower. This is due to the added weight of the mast and the higher center of gravity of the SSF with the attached mast.

Figure 26 plots the various properties of the SSF against an increasing Outer Diameter. The trends seen with the mast included are the same as when there is no mast attached. However, the metacentric height and the effective metacentric height are much lower. It is interesting to note that the overall $\overline{KG}$ decreases from around 29in to around 18in. From this result, it is seen that the mast effect of lowering the effective metacentric height decreases as the outer and inner diameters of Section 4 increase.

Figure 27 plots the various properties of the SSF against a uniform increasing of all Diameters. The trends seen with the mast included are the same as when there is no mast attached. However, the metacentric height and the effective metacentric height are much lower. It is interesting

to note that the overall $\overline{KG}$ decreases from around 29in to around 20in. From this result, it is seen that the mast effect of lowering the effective metacentric height decreases as all diameters increase in a uniform manner.

RIGHTING MOMENT AND RIGHITNG LEVER ANALYSIS

This chapter presents the method for calculating both the righting moment and righting arm for the baseline SSF with a mast. It then expands that analysis to include select cases of the geometric variations presented previously. Figure 28 shows the water ballast CG and the CG of the float and their respective locations. This will illustrate the water ballast effect at more pronounced angles of heel.

All properties in this section were calculated using data obtained from the solid model of the SSF. A plane was oriented parallel to the **xOy** plane at a vertical height equal to the calculated draught. This plane was then rotated and the mass, volume, and location properties above and below the plane were taken. From this, the centers of gravity and buoyancy were found with respect to the fixed-SSF frame.

It is assumed that the added mass below the waterline does not significantly affect draught. This allows the center of rotation to remain at O and also serve as the center of flotation. A full range of heel angles were analyzed, from level to the air entrance angle, because of this the small angle assumptions are not valid and therefore the metacentric height is not used as a measure of stability. Instead, the righting moment and the righting lever are used to determine stability.

Figure 29 shows the maximum heel angle allowable for the baseline geometry. At 31.5° heel the inner corner of Section 1 breaches the water lines and the internal volume is no longer air tight. This nullifies the effect of the ballast water by rendering it ineffective. Because of this, the extreme value for heel angle is 31.5° for the following analysis.

Righting Moment and Righting Lever: Baseline SSF.

To simplify the equations, all calculations are performed in the earth-fixed frame. This requires that some of the data taken be rotated by the rotation matrix , $\underline{R}$ **.**

$$\underline{R} = \begin{bmatrix} \cos\phi & 0 & -\sin\phi \\ 0 & 1 & 0 \\ \sin\phi & 0 & \cos\phi \end{bmatrix} \quad \textbf{(23)}$$

Figure 30 is a free-body diagram of the baseline float heeled to an angle ϕ . The righting moment is calculated by summing the moments around the center of flotation, O.

$$\sum M_o = \left(X_{ssf} * F_{ssf}\right) + \left(X_{buoy} * F_{buoy}\right) + \left(X_{bw} * F_{bw}\right) \quad \textbf{(24)}$$

Where F_{buoy} is the buoyancy force, X_{buoy} is the horizontal distance from O to the SSF center of buoyancy, F_{bw} is the gravitational force of the ballast water, X_{bw} is the horizontal distance from O to the ballast water center of gravity, F_{SSF} is the gravitational force of the SSF without the weight of the ballast water, and X_{SSF} is the horizontal distance from O to the center of gravity of the SSF without the weight of the ballast water.

Where,

$$F_{ssf} = -W_{ssf} \quad \textbf{(25)}$$

and,

$$F_{bw} = -W_{bw} \quad \textbf{(26)}$$

and

$$\begin{aligned} F_{buoy} &= -F_{ssf} + -F_{bw} \\ \Rightarrow F_{buoy} &= -\left(-W_{ssf} + -W_{bw}\right) = W_{ssf} + W_{bw} \end{aligned} \quad \textbf{(27)}$$

Where W_{ssf} is the weight of the SSF without the ballast water, and W_{bw} is the weight of the ballast water.

Inserting Eq. (25), Eq. (26), and Eq. (27) into Eq. (24),

$$\sum M_o = \left(X_{ssf} * -W_{ssf}\right) + \left[X_{buoy} * \left(W_{ssf} + W_{bw}\right)\right] + \left(X_{bw} * -W_{bw}\right) \quad \textbf{(28)}$$

$$\Rightarrow \sum M_o = W_{ssf}\left(X_{buoy} - X_{ssf}\right) + W_{bw}\left(X_{buoy} - X_{bw}\right) \quad \textbf{(29)}$$

Looking at Eq. (29) conclusions about the heeling moment become evident. It is known that X_{bw} always lies in the negative X-direction. Likewise, X_{ssf} and X_{buoy} always lie in the positive X-direction. The quantity $W_{ssf}\left(X_{buoy} - X_{ssf}\right)$ remains positive for the following condition: $X_{buoy} > X_{ssf}$. Also, the quantity $W_{bw}\left(X_{buoy} - X_{bw}\right)$ remains positive for all values of X_{buoy} and X_{bw}.

The righting moment will increase until $X_{buoy} > X_{ssf}$ and then it will decrease. Once the righting moment begins to decrease it will remain positive while the following condition is true:

$$W_{bw}\left(X_{buoy} - X_{bw}\right) > W_{ssf}\left(X_{buoy} - X_{ssf}\right) \quad \textbf{(30)}$$

If the left hand side of Eq. (30) becomes greater than the right hand side before air is allowed to enter into the internal volume, the righting moment becomes negative and the SSF capsizes.

Figure 31 plots the righting moment against the heel angle. The maximum heeling moment of 215.30in-lbs occurs at a heel angle of 8°. Beyond this heel angle, the SSF will lose its power to return to equilibrium. It is interesting to note that the value of the righting moment becomes negative at 26.5°, which means the angle of vanishing stability occurs at a lower angle of heel than the entrance of air into the internal volume.

The righting lever, $\overline{GZ}$, as shown in Figure 32, is the horizontal distance between the total center of gravity of the SSF and the center of buoyancy, B'. As long as the value of $\overline{GZ}$ is positive the righting moment remains positive.

$$\overline{GZ} = X_{buoy} - X_{OG} \quad \textbf{(31)}$$

Figure 33 plots X_{buoy}, X_{OG}, and $\overline{GZ}$ against the heel angle. Note that the shape of the righting lever curve follows the same trend as that of the righting moment curve. The water ballast mass changes with every angle of heel, so its effect is to increase the righting moment. This added ballast weight increases the righting effect of the ballast water as the heel angle increases.

In Figure 31 and Figure 33, the curves for the righting moment and the righting lever have similar trends. Between 3° and 5°, there is a linear ramp up where the righting moment and lever are relatively small in comparison to the maximum values. Between these angles the value of $\overline{GM}$ stays relatively constant. On a ship, in general, this range has an upper limit between 10° and 12°. For a SSF the range where the value of $\overline{GM}$ can be used as a measure of stability is decreased. The reason for this lies in the materials used in the construction of the SSF.

As shown in Figure 34, between 3° and 5° the moments of inertia of both the SSF and the ballast water remain constant. This is because the only portion of the SSF below the waterline is the float body, which is constructed of the low-density polyurethane foam. This keeps the center of buoyancy relatively close to the centerline of the SSF and the effect of the heeling angle small. In this range, the metacentric height doesn't change significantly.

Next, there is a sharp rise between 3° and 5° where the righting moment and lever increases sharply. This increase is an effect of the higher density acrylic top plate of the SSF falling below the waterline, which submerges a higher density component further from the center of flotation. This shifts the center of buoyancy, X_{buoy}, further in the positive X-direction and increases the righting

moment. When correlated to Figure 34, it is seen that in this range of heel angles the moment of inertia for the ballast water begins to decreases sharply, while the SSF moment of inertia remains constant.

Following the sharp rise, there is a non-linear section between 5° and 15° where the righting moment reaches its maximum value and begins to decrease. In Figure 33, the curve for X_{OG} transitions from a negative value to a positive value between 6° and 7°. Referring to Eq. (29), this results in a decreasing value of $\overline{GZ}$, which also means a decrease in the righting moment.

In the last section of the curve, from 15° to 31.5°, the righting moment decreases until it reaches a negative value at 26.5°. In this range, the values for X_{OG} increase at an almost linear rate, while the values of X_{buoy} decrease non-linearly at a much less pronounced rate than the value of X_{OG} increases, which means the center of buoyancy is not changing as fast as the SSF center of gravity. It also shows that the heeling moment of the center of gravity of the SSF, not including the ballast water, has more of an effect than the righting moment of the ballast water and the buoyancy force. Referring to Eq. (29), shows that this offset will result in a decreasing value of $\overline{GZ}$ decreasing.

Comparison: Non-SSF and SSF.

Once again, it is important to compare the result of the float with suction-stabilization to that of a float that does not utilize suction-stabilization. Figure 35, shows a marked increase in the righting moment of the SSF versus the Non-SSF. The Non-SSF reaches a maximum righting moment of 19.63in-lbs at a heel angle of 4.5°. This is 90.8% lower than that of the SSF.

Figure 36, shows a marked increase in the righting lever of the SSF versus the Non-SSF. The Non-SSF has a maximum righting lever of .798in at a heel angle of 4.5°. This is 84.2% lower than that of the SSF. At 10°, in both Figure 35 and Figure 36, there is a slight increase in the righting moment, not enough to make it stable, but enough to stand out on the plot. This increase is due to the higher density top plate of the Non-SSF being submerged below the waterline and increasing the

value of X_{buoy}. Figure 35 and Figure 36 clearly show that adding Suction-Stabilization to a float dramatically increases the stability of the float.

Righting Moment and Righting Lever: Parametric studies.

Geometry and design influence the hydrostatic and hydrodynamic characteristics of the SSF. To understand the exact ways that geometry effect the stability of the SSF, six geometric variations were analyzed in the same manner as the baseline SSF and then compared to the baseline SSF by their respective Righting Arms and Righting Levers.

a) Geometry Variation: Section 4 Height.

Figure 37 gives a pictorial representation of the two Section 4 heights, used to compare the effect of Section 4 height on both the righting moment and the righting lever.

Table 9 gives a comparison of the various properties of the two Section 4 heights against the baseline geometry.

Figure 38 plots the righting moment for the two Section 4 Heights against the heel angle. The righting moment for the baseline SSF is plotted in black for comparison. The righting lever reaches a maximum value of 215.30in-lbs at 8° when Section 4 height is 1.50in, a value of 231.32in-lbs at 10° when Section 4 height is 2.75in**,** and a value of 243.52in-lbs at 12° when Section 4 height is 4.00in.Increasing the height of Section 4, appears to keep the righting moment at a higher value for more degrees of heel.

The righting moment is greater than 150in-lbs for a range of at $4.5^\circ - 15.5^\circ$ when Section 4 height is 1.50in, for a range of at $5^\circ - 16^\circ$ when Section 4 height is 2.75in**,** and for a range of at $6.5^\circ - 25.5^\circ$ when Section 4 height is 4.00in. From this, it is apparent that greater the height of section 4, larger the range of heel angles that will have a large heeling moment. This means that the float will have an increased tendency to return to equilibrium. However, this must be weighed against the lowered metacentric height and increased roll period.

Figure 39 plots the righting lever for the two Section 4 Heights against the heel angle. The righting lever for the baseline SSF is plotted in black for comparison. It is observed that the peak values of the righting moment are all similar, but the maximum values for the righting lever are not similar. The righting lever reaches a maximum value of 5.044in at 8° when Section 4 height is 1.50in, a value of 4.984in at 11° when Section 4 height is 2.75in**,** and a value of 4.849 at 12° when Section 4 height is 4.00in.

b) Geometry Variation: Section 4 Diameters.

Figure 40 gives a pictorial representation of the two outer diameter variations used to compare the effect of outer diameter on both the righting moment and the righting lever. Table 10 gives a comparison of the various properties of the two outer diameter geometries against the baseline geometry.

Figure 41 plots the righting moment for the two Section 4 diameters against the heel angle. The righting moment for the baseline SSF is plotted in black for comparison. There is a large disparity between the curves. The righting moment peaks at a value of 215.30in-lbs at 8° when the outer diameter of Section 4 is 30in and the inner diameter of Sections 1 & 2 is 19in, at a value of 481.36in-lbs at 11° when the outer diameter of Section 4 is 35in and the inner diameter of Sections 1 & 2 is 19in, and at a value of 857.58in-lbs at 11° when the outer diameter of Section 4 is 40in and the inner diameter of Sections 1 & 2 is 19in.

Figure 42 plots the righting lever for the two outer diameter variations against the heel angle. The baseline geometry is plotted for a comparison. The righting lever reaches a maximum at a value of 5.044in at 8° when the outer diameter of Section 4 is 30in and the inner diameter Sections 1 & 2 is 19in, at a value of 7.971in at 12° when the outer diameter of Section 4 is 35in and the inner diameter Sections 1 & 2 is 19in**,** and at a value of 10.735in at 10° when the outer diameter of Section 4 is 40in and the inner diameter Sections 1 & 2 is 19in.

The righting moment and lever curves end abruptly at 28° when the outer diameter of Section 4 is 35in and the inner diameter Sections 1 & 2 is 19in, and at 27° when the outer diameter of Section 4 is 40in and the inner diameter of Sections 1 & 2 is 19in. At these angles air is allowed to enter the internal volume. So, while the righting moment is larger than the baseline geometry increasing the diameter to gain stability limits the range of allowable heeling angles.

c)Geometry Variation: All Section Diameters.

Figure 43 gives a pictorial representation of the two diameter variations used to compare the effect of diameter on both the righting moment and the righting lever.

Table 11 gives a comparison of the various properties of the two diameter geometries against the baseline geometry.

Figure 44 plots the righting moment for the two diameter variations against the heel angle. The baseline geometry is plotted for a comparison. There is a large disparity between the curves. The righting moment peaks at a value of 215.30in-lbs at 8° when the outer diameter of Section 4 is 30in and the inner diameter of Sections 1 & 2 is 19in, at a value of 420.64in-lbs at 10° when the outer diameter of Section 4 is 35in and the inner diameter of Sections 1 & 2 is 24in**,** and at a value of 689.02in-lbs at 11° when the outer diameter of Section 4 is 40in and the inner diameter of Sections 1 & 2 is 29in.

Figure 45 plots the righting lever for the two diameter variations against the heel angle. The baseline geometry is plotted for a comparison. The righting lever reaches a maximum at a value of 5.044in at 8° when the outer diameter of Section 4 is 30in and the inner diameter of Sections 1 & 2 is 19in, at a value of 8.111in at 10° when the outer diameter of Section 4 is 35in and the inner diameter of Sections 1 & 2 is 24in**,** and at a value of 11.087in at 10° when the outer diameter of Section 4 is 40in and the inner diameter of Sections 1 & 2 is 29in.

The righting moment and lever curves end abruptly at 24° when the outer diameter of Section 4 is 35in and the inner diameter of Sections 1 & 2 is 24in, and at 20° when the outer diameter of Section 4 is 40in and the inner diameter of Sections 1 & 2 is 29in. At these angles air is allowed to enter the internal volume. So, while the righting moment is larger than the baseline geometry increasing the diameter to gain stability limits the range of allowable heeling angles.

d) Comparison: all Geometric Variations.

Figure 46 plots the righting lever for all the geometric variations and

Table 12 lists the maximum righting moments of the various geometries in ascending order. Figure 47 plots the righting lever against the heel angle for all the geometric variations and Table 13 lists the maximum righting levers of the various geometries in ascending order. It is interesting to note that the length of the righting arm is not an exact indicator of the righting moment. For example, the righting lever is 5.044in for the baseline geometry, while the length of the righting lever is 4.849in when the height of Section 4 is 4.00in.

This, however, does not imply that the righting moment follows a similar trend. Looking at

Table 12, the value of the righting moment is 215.30in-lbs for the baseline geometry, while the value of the righting moment is 243.52in-lbs when the height of Section 4 is 4.00in. This is a result of the increased height of Section 4, which increases the weight of the trapped water and creates a larger righting moment for a shorter righting lever length.

Table 14 lists the angles of vanishing stability and the air entrance angles for the seven SSF Geometries. The baseline geometry and the geometries with increased Section 4 heights have an angle of vanishing stability that is less than the air entrance angle. Increasing the diameters, both the Section 4 diameters alone and all diameters equally, eliminates the angle of vanishing stability, because it significantly decreases the air entrance angle. At first glance, this may appear as a negative, however when the increased righting moment is taken into account it is more beneficial to decrease the air entrance angle in order to increase the righting moment and stability.

EXPERIMENTAL DATA

A simple Experimental SSF (ESSF), as shown in Figure 48, was tested in a backyard pool to verify the calculations of hydrostatic properties and also the behavior of the SSF with a mast in practically. This test was not rigorous and meant as a qualitative check on some of the analyses presented in this study.

Table 15 presents the properties for the Experimental SSF (ESSF). All properties were calculated using the density of fresh water rather than the density of salt water. Fresh water is slightly denser than fresh water, which decreases the displaced volume and draught. Due to construction issues, the ESSF used a smaller mast, as compared to the one used in the analysis. Still, correlations are possible and trends could be verified

According to calculations, and as observed in Table 15, the draught, $T = 5.634in$. A ruler was attached to the side of the ESSF to check draught when submerged. This ruler measures vertically down from the top of the ESSF, so as to verify the draught .The draught is subtracted from the total height of the ESSF.

$$H_{WL} = H_{TOTAL} - T$$
$$H_{WL} = 6.875in - 5.634in = 1.241in$$

Figure 49 shows the actual draught of the ESSF, which is just above 1.39in. The disparity in calculated draught and actual draught is a combination of a slight bend in the mast, which caused the ESSF to list away from the side with the tape measure, and the motion of the water in the pool.

The ESSF was then heeled to an angle of 22°, as shown in Figure 50, and allowed to roll back to equilibrium. First, the ESSF rolled past equilibrium and reached a heel angel of $\sim -9^\circ$, as shown in Figure 51. It then rolled three more times at low heel angles, between -3° and 3°, before damping out at 0°. Due to the bend in the mast, the ESSF was unable to return to equilibrium when heeled past 24° which is close to the predicted value of 26.5° in Table 14.

CONCLUSION

When a float platform incorporates Suction-Stabilization there is a dramatic improvement in stability. Suction-Stabilization raises the effective metacentric height by approximately 300% and it increases the righting moment and lever between 1000% and 1100% above a float with the same geometry that does not incorporate Suction-Stabilization. The increase in these metrics allows the SSF to withstand higher wind and wave loads than it would in the absence of Suction-Stabilization.

Looking at Table 16, we can conclude that the overall stability of the baseline SSF is improved slightly when the height of Section 4 is increased, although at the cost of a lower metacentric height. The reason the decreased metacentric height does not decrease the stability is that the increased Section 4 height allows for a greater volume of trapped ballast water and increases the IST effect.

Stability increases dramatically with the increase of the Section 4 outer and inner diameters and even more so with the increase of the inner and outer diameters of all sections. However, with the increase of any diameter, without an appropriate height change, comes the adverse effect of

decreasing the air entrance angle and limiting the operable heel angle range. This limit in operable heel angle range is offset by the increased righting moment and righting lever, which requires a much higher load to attain larger heel angles. Suction stabilization also improves the dynamic stability and the hydrodynamic analysis of SSF under wind and wave loading will be presented in another journal article.

NOMENCLATURE

$\overline{GM}$	Metacentric height
$\overline{GZ}$	Righting lever
φ	Heel angle
M_R	Righting moment
W_{ship}	Weight of the ship
ℓ_k	Value of stability cross curves

$\overline{KG}$	Vertical distance between the bottoms-most point on the ship and the ship center of gravity
α	Air entrance angle
φ_{VS}	Angle of vanishing stability
$\overline{BM}$	Metacentric radius
$\overline{KB}$	Distance from the base point (K) to the center of buoyancy
I_{wp}	Area Moment of Inertia of the water plane
V_{dis}	The total volume displaced
I_{bS4}	Area Moment of Inertia of the SSF body in Section 4
I_{wS4}	Area Moment of Inertia of the water in SSF at Section 4
T	Draught
$\overline{KG_t}$	Centre of gravity of the assembly
$\overline{KG_b}$	Centre of gravity of the base SSF
m_b	Total mas of the SSF
$\overline{KG}_{ballast}$	Centre of gravity of the ballast water in SSF
$m_{ballast}$	Total mass of the ballast
m_{bbWP}	Mass of the SSF below the water line
H_{bbWP}	Height of the SSF below the water line
H_{S1}	Height of section 1
m_{bS1}	Mass of SSF base in section 1
H_{S2}	Height of section 2
m_{bS2}	Mass of SSF base in section 2

H_{S3}	Height of section 3
m_{bS3}	Mass of SSF base in section 3
ξ	Total height until section 3
A_{bS4}	Area of SSF base in section 4
ρ_b	Density of SSF base material
ρ_{SW}	Density of salt water
l_F	Raised metacentric height
I_{w4}	Area Moment of Inertia at Section 4
$\overline{GM}_{eff}$	Effective metacentric height
A_{bi}	Area of SSF base of ith section
A_{si}	Area of SSF of ith section
H_{bi}	Height of SSF base in each section
H_{Si}	Height of each section
ρ_{SW}	Density of salt water
V_{bSi}	Volume of SSF base in each section
g	Gravitational constant
D_O	Outer diameter of the float
P_{roll}	Natural roll period of the float
ω_{roll}	Natural angular frequency of free roll of the SSF
i_m	Mass radius of gyration
KG_{mast}	Center of gravity of mast
H_{mast}	Height of mast

H_{body}	Total height of the SSF body
X_{ssf}	Horizontal distance from O to the center of gravity of the SSF without the weight of the ballast water
F_{ssf}	Gravitational force of the SSF without the weight of the ballast water
X_{buoy}	Horizontal distance from O to the SSF center of buoyancy
F_{buoy}	Buoyancy force
X_{bw}	Horizontal distance from O to the ballast water center of gravity
F_{bw}	Gravitational force of the ballast water
W_{ssf}	Weight of the SSF without the ballast water
W_{bw}	Weight of the ballast water
H_{WL}	Depth of water level from the top surface of the SSF

REFERENCES

[1] Biran, Adrian ,2003, *Ship Hydrostatic and Stability.* Oxford: Butterworth-Heinemann (Elsevier).

[2] Butterfield S., Jonkman J., Musial W., Sclavounos P.D. and Wayman. E.N., 2006, "Coupled Dynamics Modeling of Floating Wind Turbine Systems." *Offshore Technological Conference No. NREL/CP-500-39481.*

[3] Butterfield S., Jonkman J., Musial W., Sclavounos P.D. and Wayman. E.N. ,2007. "Coupled Dynamics Modeling of Floating Wind Turbine Systems." *Offshore Technological Conference No. NREL/CP-500-38116.* 3-7.

[4] Cheung, K.F., Lee, S.K., Phadke, A.C., Seidl, L.H., Smith, D.A. ,2000, "Hydrodynamic Response of a Pneumatic Floating Platform." *Ocean Engineering. 27, 1407-1444* 1.

[5] Kliava, Janis, Megel, Jacques., 2010, "Metacenter and Ship Stability." *American Journal of Physics. 78, 738-747.*

[6] Montgomery, James ,2011, Suction Stabilized Floats. United States of America Patent 13/242,489. September 23.

[7] Perunovic, Vidac, 2011, "Influence of the GZ Calculation Method on Parametric Roll Prediction." *Ocean Engineering. 38, 295-303* 1-2.

[8] Redkar, S. ,2012, "Suction Stabilisation Float-Progress Report." Mesa, Arizona, December 21

[9] Cheung, K.F., Lee, S.K., Phadke, A.C., Seidl, L.H., Smith, D.A. ,2000, "Hydrodynamic Response of a Pneumatic Floating Platform." *Ocean Engineering. 27, 1407-1444* 1.

[10] Bangun, E.P.,Utsonomiya, T., Wang, C.M., 2010, "Hydrodynamic Forces on a Rolling Barge with Bilge Keels " *Ocean Engineering. 32, 219-232*.

[11] Taylor, Metin , 2007, “Parametric Resonance of Container Ships.” Ocean Engineering 34, 1021-1027.

[12] Jacques M., Kliava J., 2010, “Metacenter and Ship stability”, *American Journal of Physics 78,738.*

[13] Lee S.K., 2000, “Stability Analysis of an Initially Inclined Ship in Following Sea”, *Journal of Applied Mechanics ASME 67(4),717-719.*

Figure Captions List

Figure 1	General SSF
Figure 2	Cross-sectional view of general SSF
Figure 3	Baseline SSF geometry with top (section5) removed

Figure 4	Cross-section of baseline SSF
Figure 5	Definition of coordinate system
Figure 6	Section 4 height limits
Figure 7	Draught vs. Section 4 height
Figure 8	Displaced volume vs. Section 4 height
Figure 9	Hydrostatic properties vs. Section 4 height
Figure 10	Section 4 outer and inner diameter limits
Figure 11	Draught vs. Section 4 diameters
Figure 12	Displaced volume vs. Section 4 diameters
Figure 13	Hydrostatic properties vs. Section 4 diameters
Figure 14	All outer and inner diameter limits
Figure 15	Draught vs. All diameters
Figure 16	Displacement volume vs. All diameters
Figure 17	Hydrostatic properties vs. All diameters
Figure 18	Pictorial representation of mast geometry
Figure 19	Draught vs. Mast weight
Figure 20	Metacentric height vs. Mast weight (up to 35lbs).
Figure 21	Metacentric height vs. Mast weight (up to 33lbs).
Figure 22	Kempf factor vs. Mast weight (up to 33lbs).
Figure 23	Metacentric height vs. Kempf kfctor.
Figure 24	SSF with mast at heel.
Figure 25	Hydrostatic properties vs. Section 4 heights.
Figure 26	Hydrostatic properties vs. Section 4 diameters.
Figure 27	Hydrostatic properties vs. All diameters
Figure 28	SSF with mast at heel.
Figure 29	Forces on SSF with mast at heel.
Figure 30	Suction-stabilized float with mast at any heel angle.

Figure 31	Righting moment vs. Heel angle for baseline SSF.
Figure 32	Righting lever diagram.
Figure 33	Righting lever vs. Heel angle for baseline SSF.
Figure 34	Water plane moment of inertia vs. Heel angle
Figure 35	Comparison of non-SSF and SSF righting moment.
Figure 36	Comparison of non-SSF and SSF righting lever.
Figure 37	Section 4 height variations.
Figure 38	Righting moment vs. Heel angle for varying Section 4 heights.
Figure 39	Righting lever vs. Heel angle for varying Section 4 heights.
Figure 40	Section 4 diameter variations.
Figure 41	Righting moment vs. Heel angle for varying Section 4 diameters.
Figure 42	Righting lever vs. Heel angle for varying Section 4 diameters.
Figure 43	All section diameter variations
Figure 44	Righting moment vs. Heel angle for varying all section diameters.
Figure 45	Righting lever vs. Heel angle for varying all section diameters.
Figure 46	Righting moment vs. Heel angle for all geometric variations
Figure 47	Righting lever vs. Heel angle for all geometric variations.
Figure 48	Experimental SSF
Figure 49	Actual draught of experimental SSF.
Figure 50	Heeled experimental SSF
Figure 51	Roll amplitude for baseline SSF heeled to 22 degree

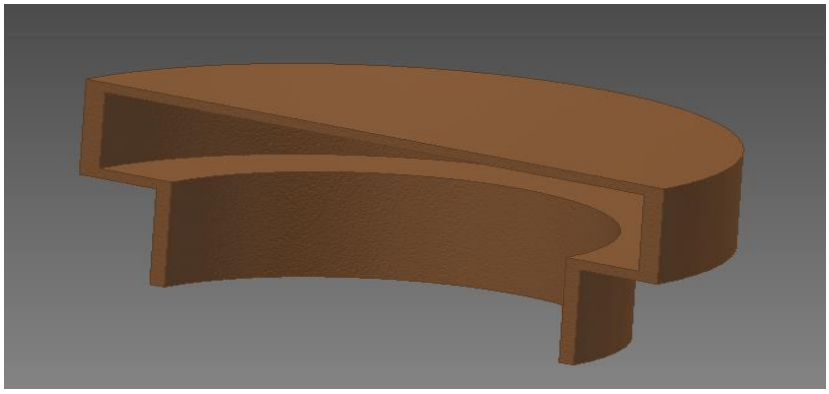

Figure 1.General SSF

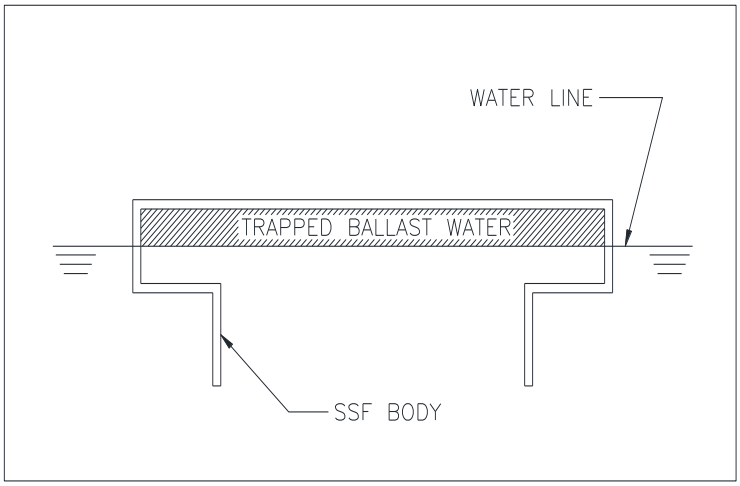

Figure 2. Cross-sectional view of general SSF

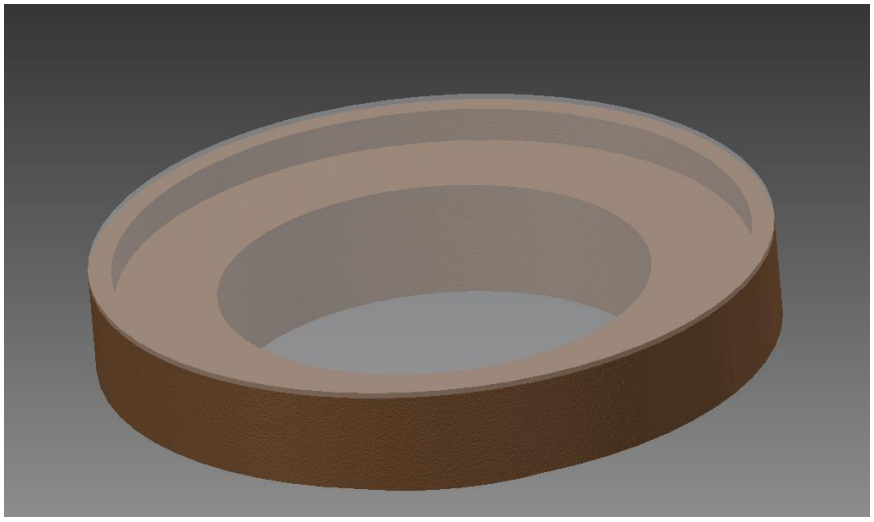

Figure 3. Baseline SSF geometry with top (section5) removed

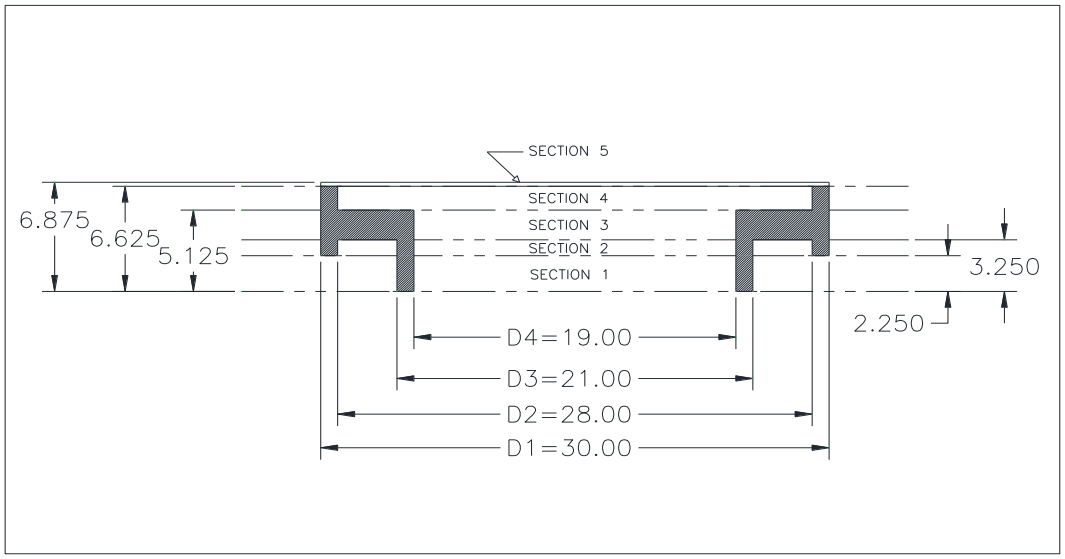

Figure 4. Cross-section of baseline SSF

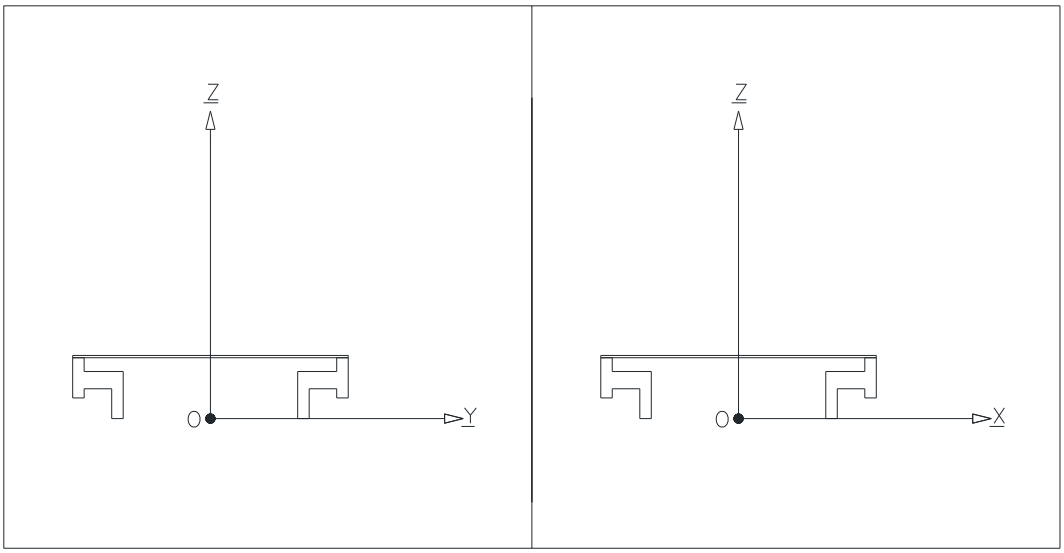

Figure 5. Definition of coordinate system

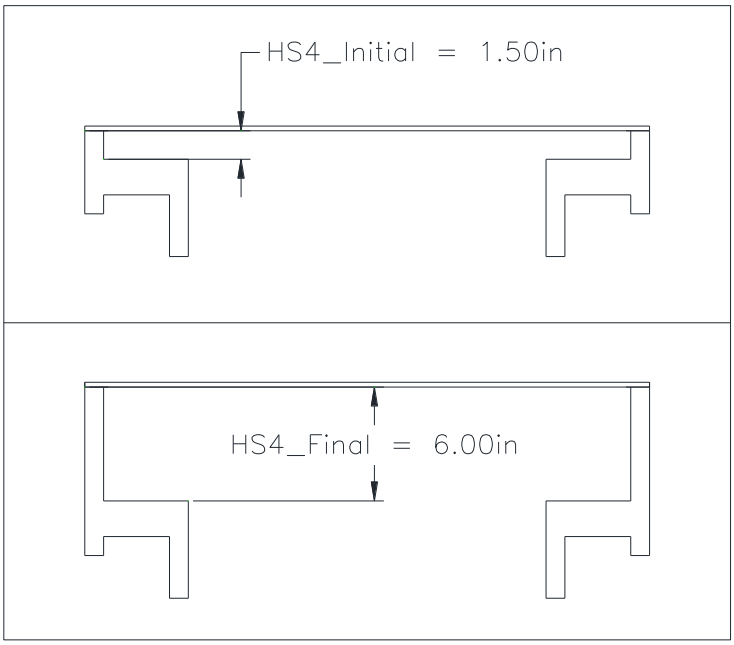

Figure 6. Section 4 height limits

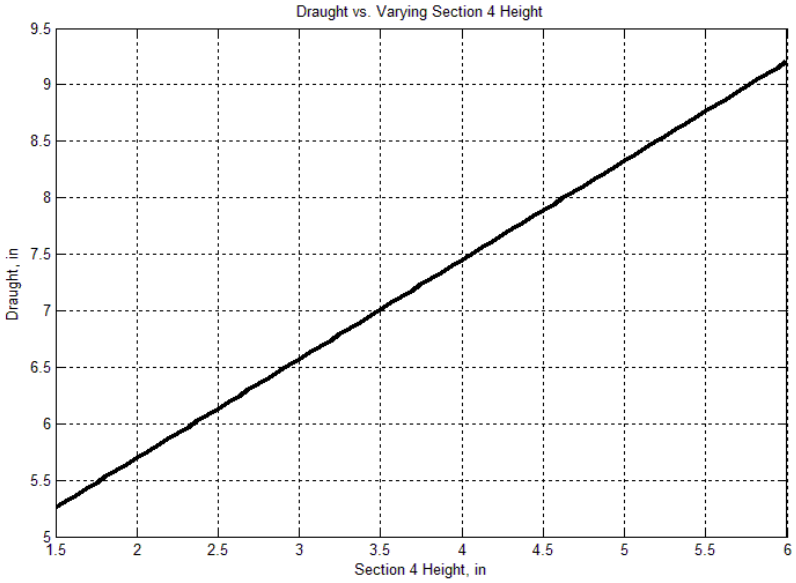

Figure 7. Draught vs. Section 4 height

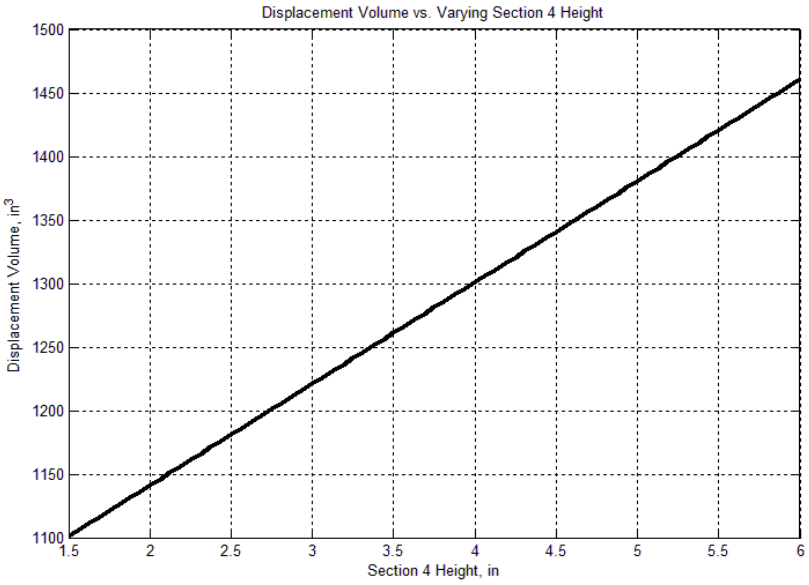

Figure 8. Displaced volume vs. Section 4 height

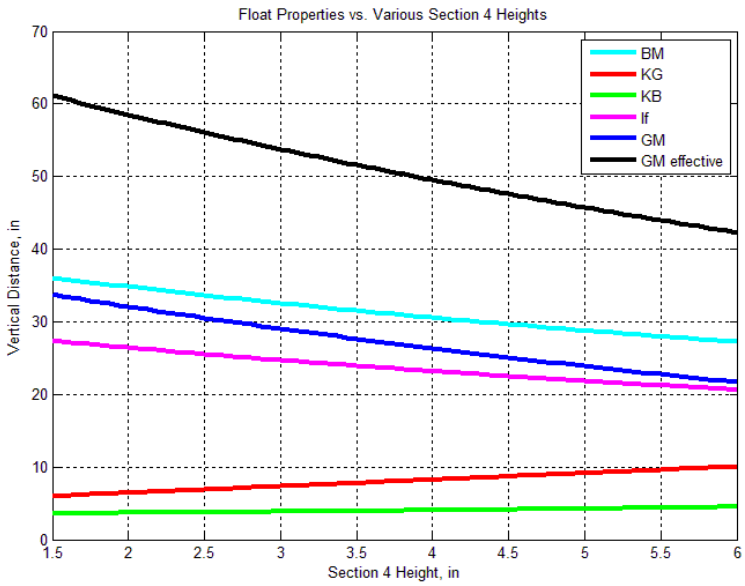

Figure 9. Hydrostatic properties vs. Section 4 height

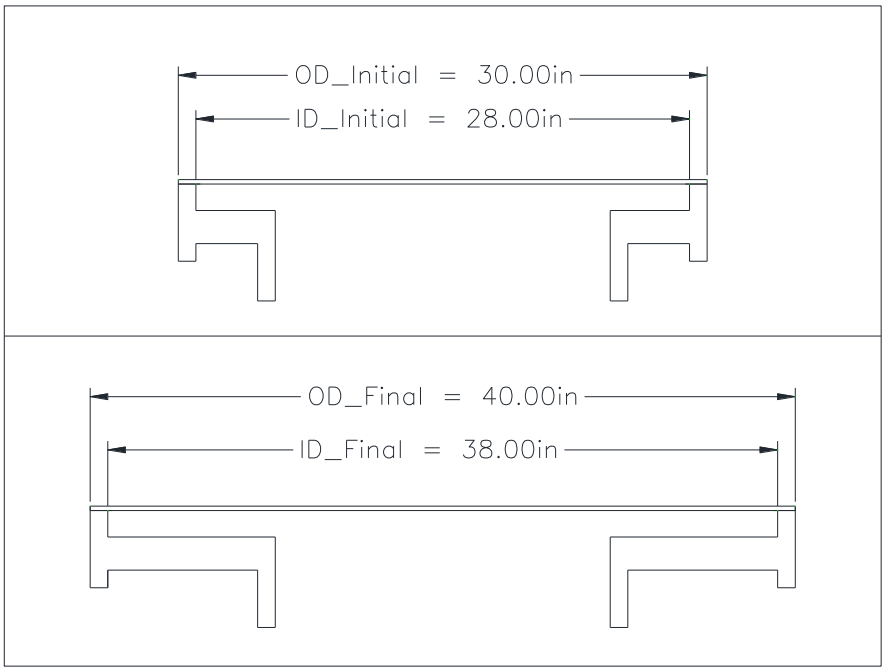

Figure 10. Section 4 outer and inner diameter limits

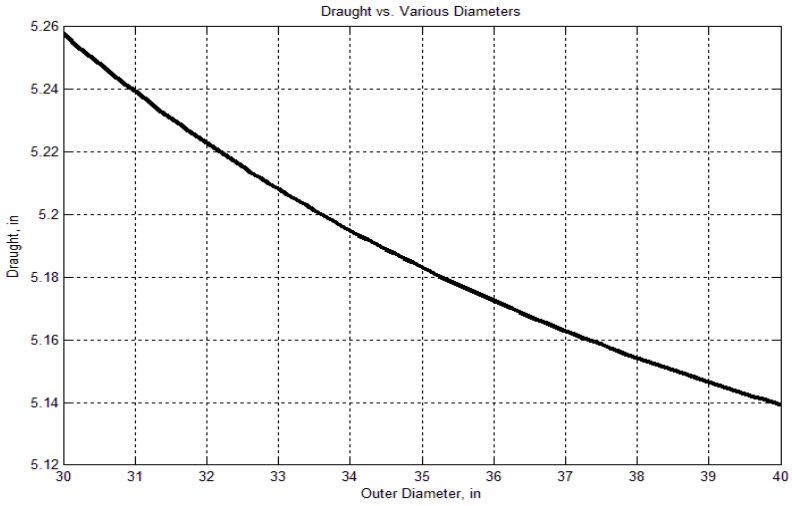

Figure 11. Draught vs. Section 4 diameters

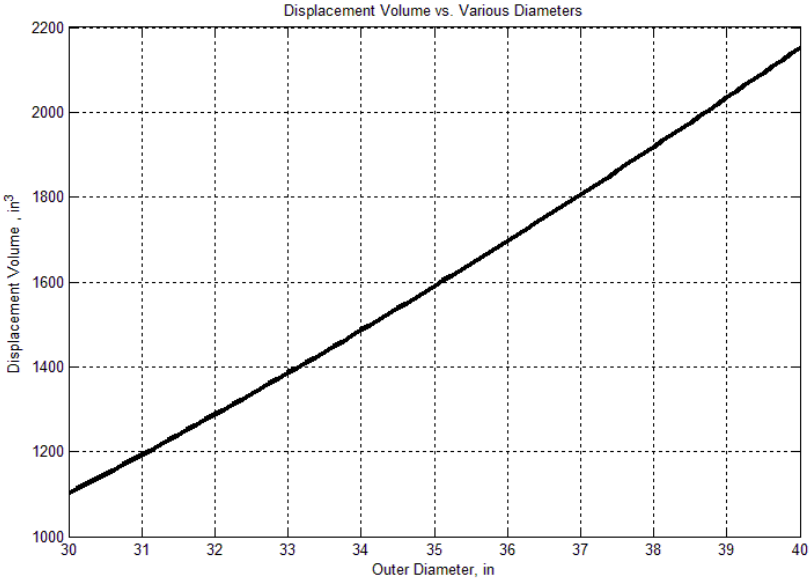

Figure 12. Displaced volume vs. Section 4 diameters

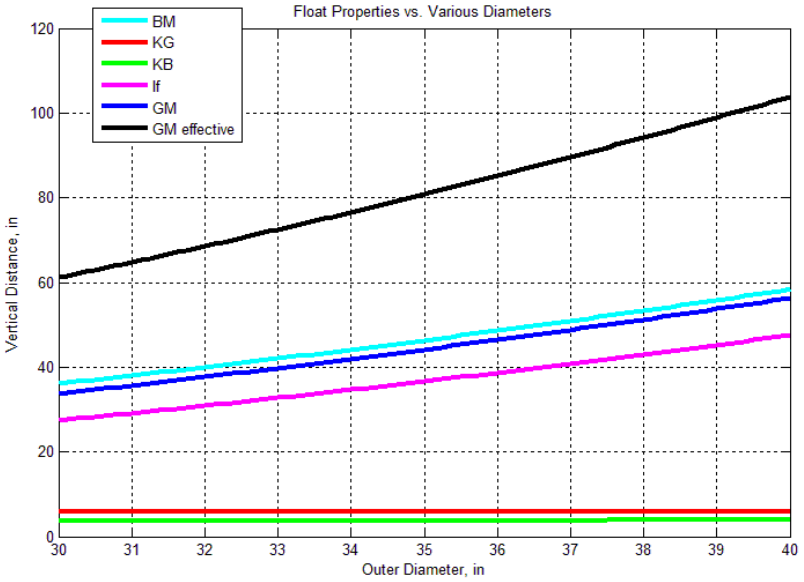

Figure 13. Hydrostatic properties vs. Section 4 diameters

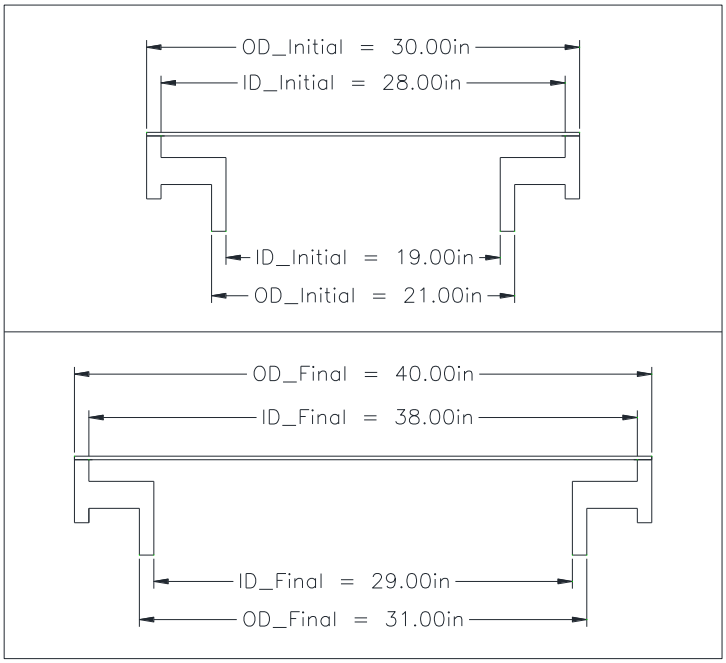

Figure 14. All outer and inner diameter limits

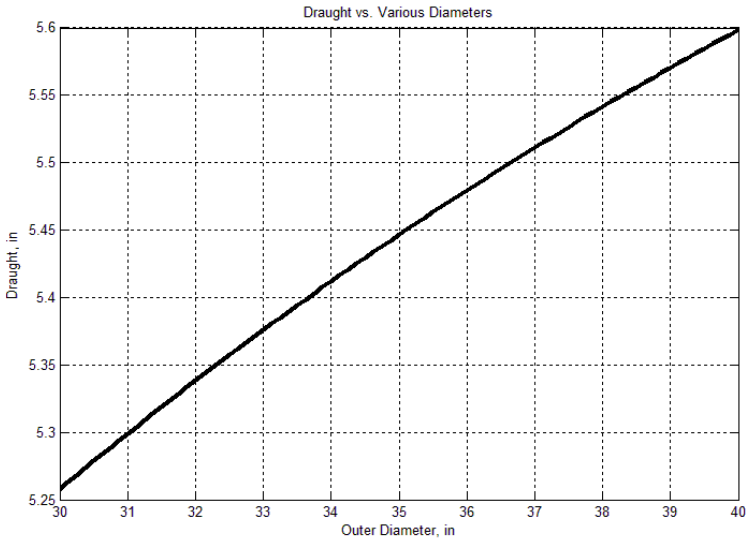

Figure 15. Draught vs. All diameters

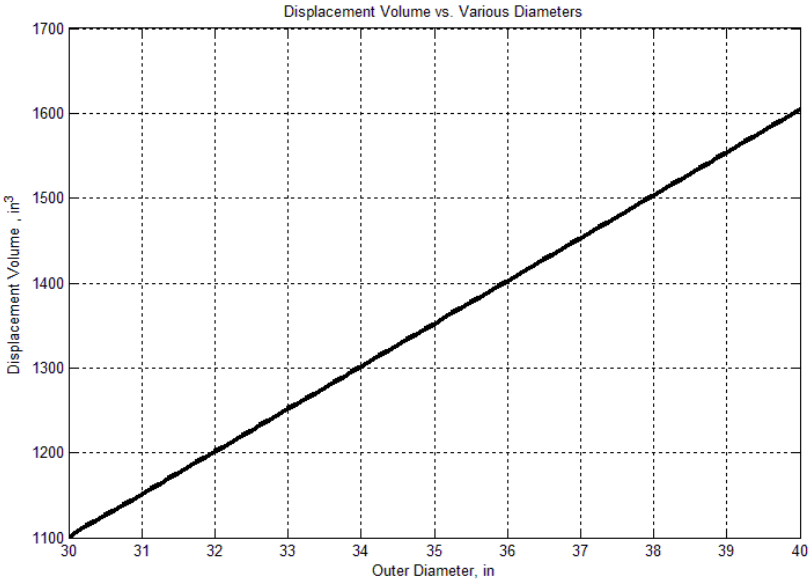

Figure 16. Displacement volume vs. All diameters

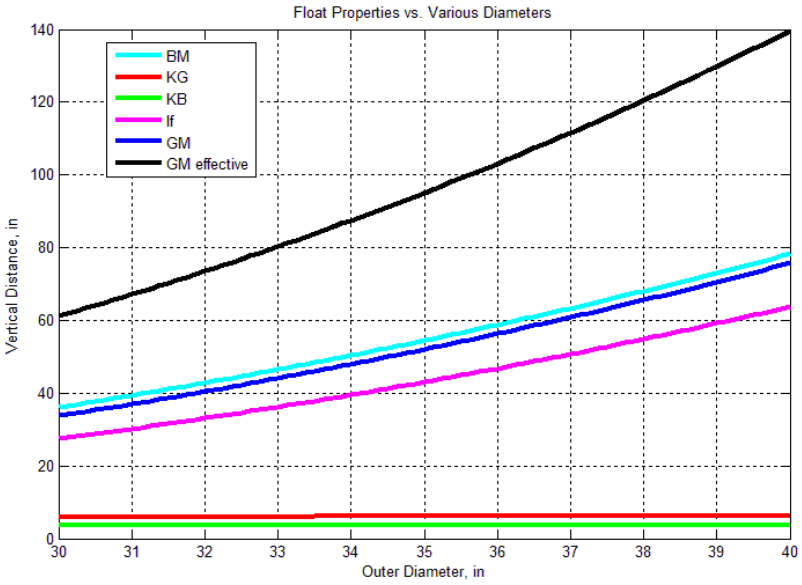

Figure 17. Hydrostatic properties vs. All diameters

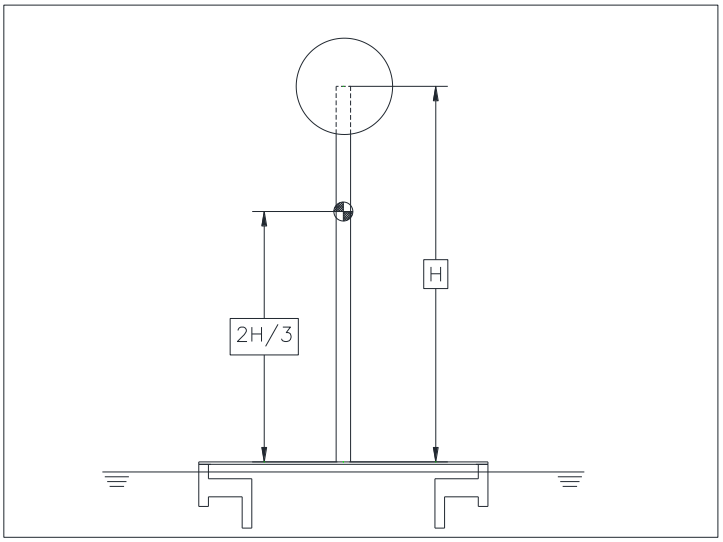

Figure 18. Pictorial representation of mast geometry

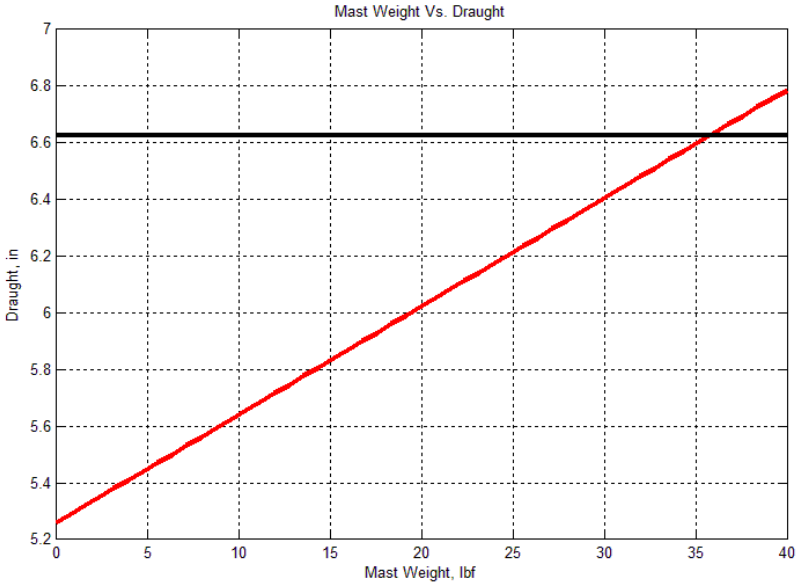

Figure 19. Draught vs. Mast weight

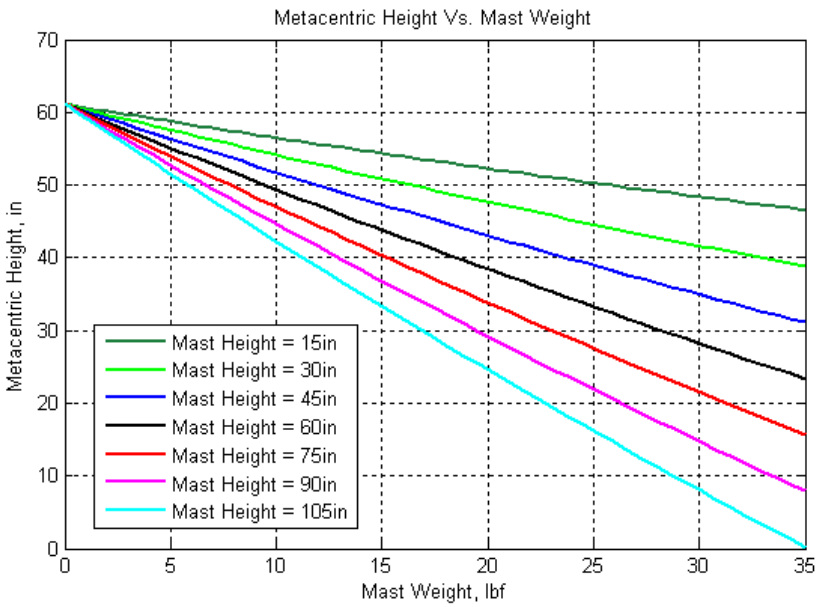

Figure 20. Metacentric height vs. Mast weight (up to 35lbs).

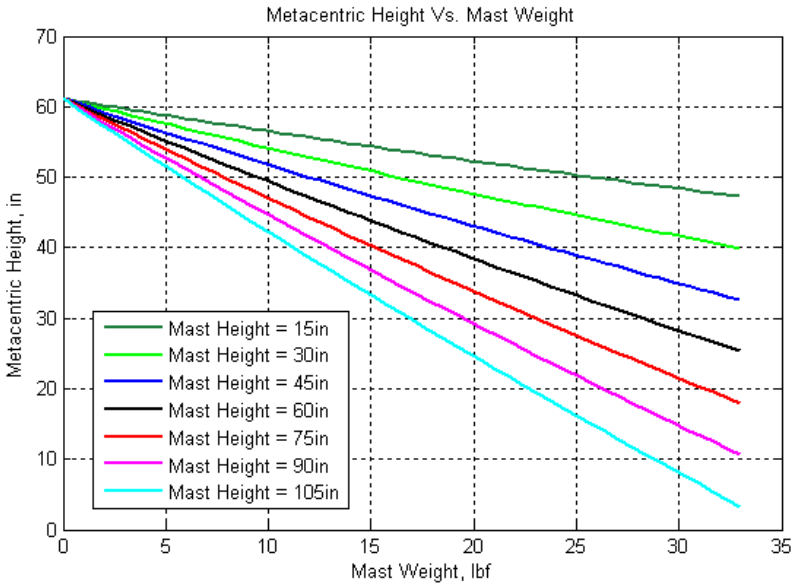

Figure 21. Metacentric height vs. Mast weight (up to 33lbs).

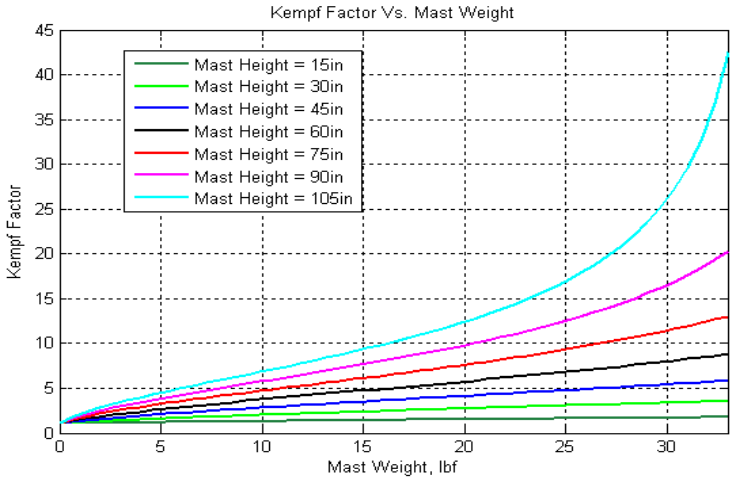

Figure 22. Kempf factor vs. Mast weight (up to 33lbs).

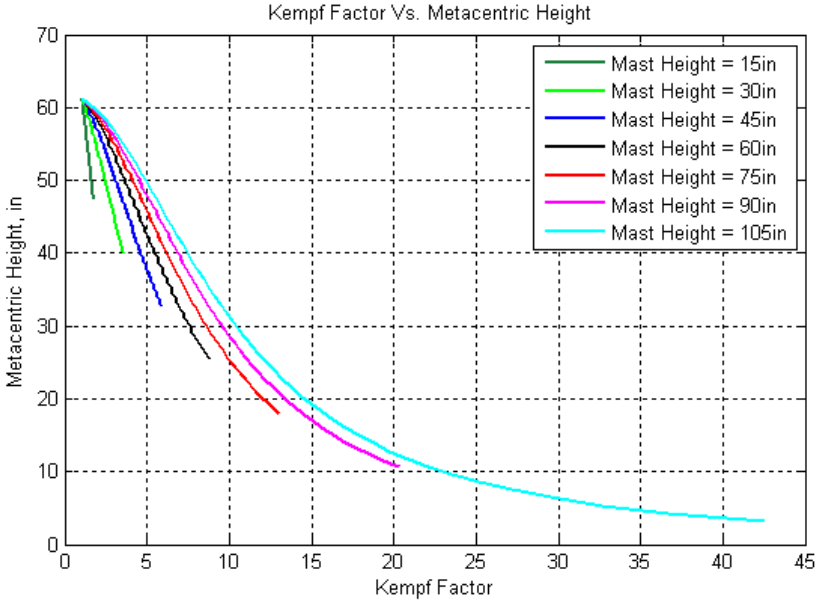

Figure 23. Metacentric height vs. Kempf factor.

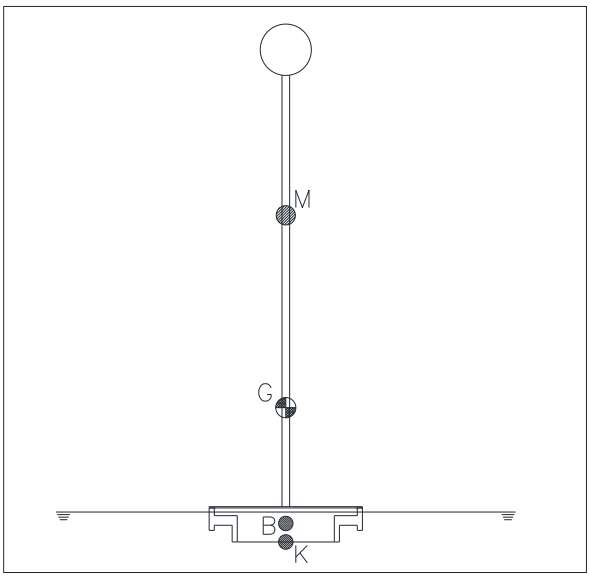

Figure 24. SSF with mast at heel.

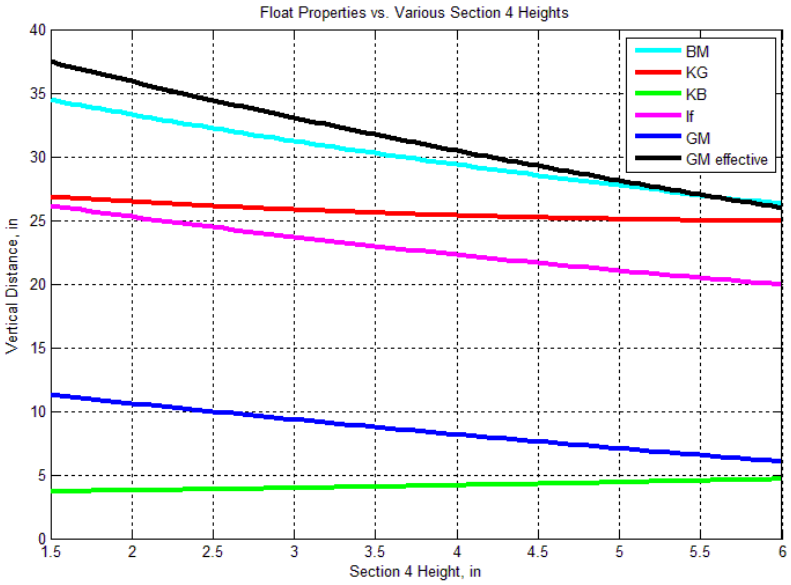

Figure 25. Hydrostatic properties vs. Section 4 heights.

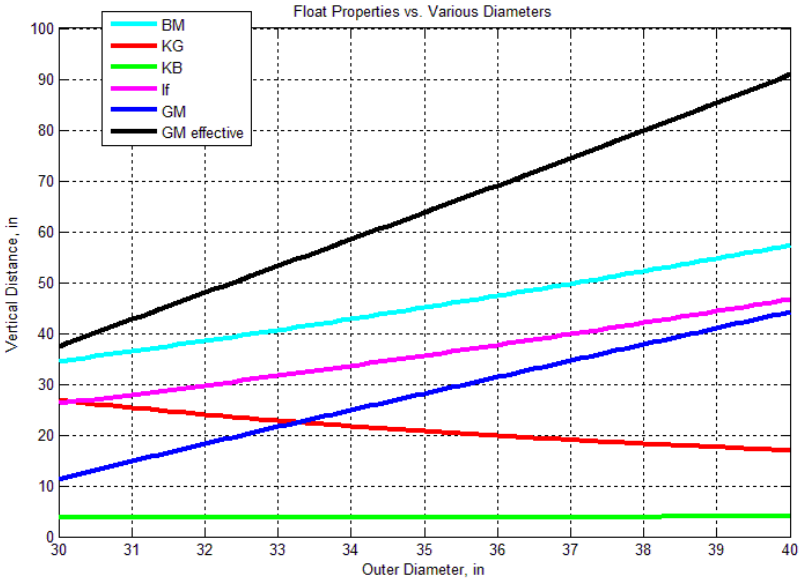

Figure 26. Hydrostatic properties vs. Section 4 diameters.

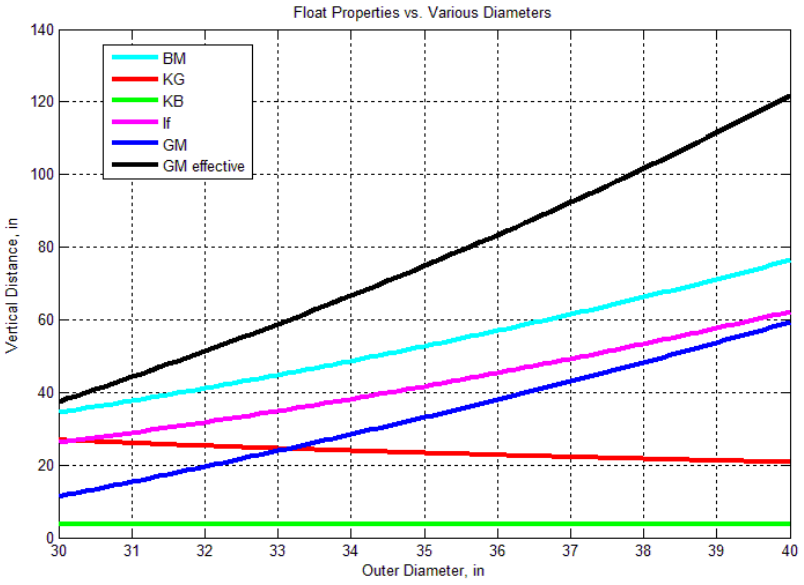

Figure 27. Hydrostatic properties vs. All diameters

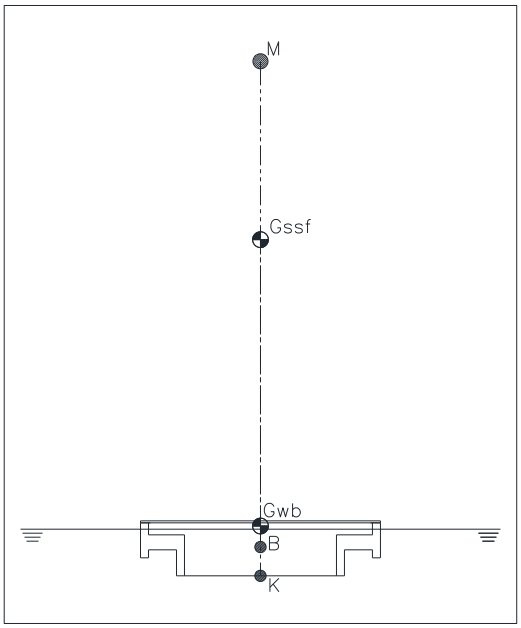

Figure 28. SSF with mast at heel.

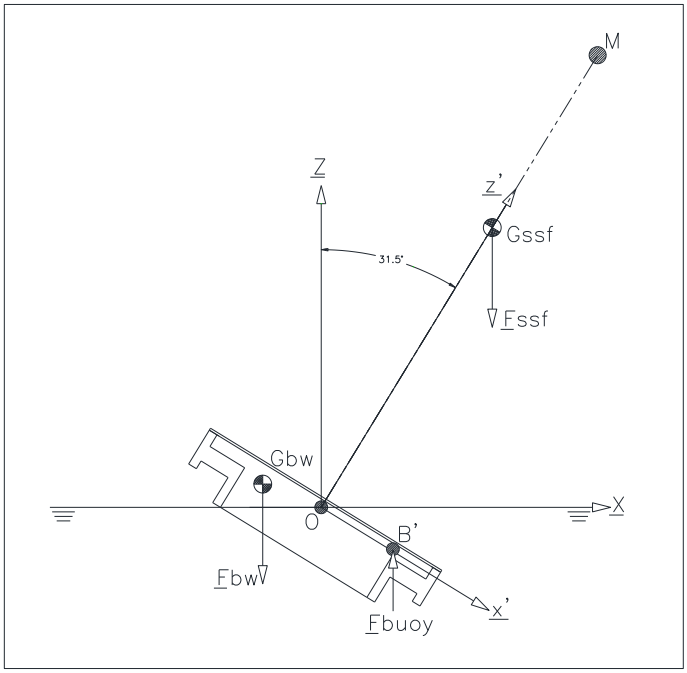

Figure 29. Forces on SSF with mast at heel.

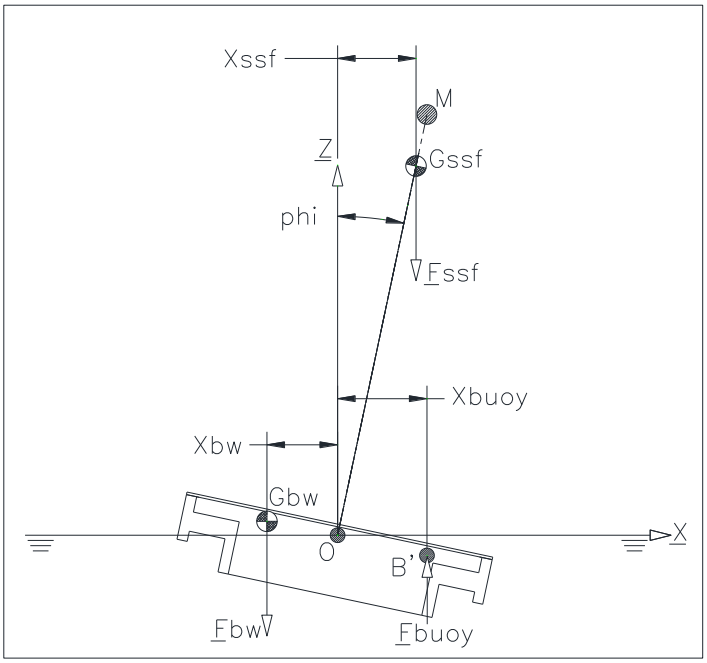

Figure 30. Suction-stabilized float with mast at any heel angle.

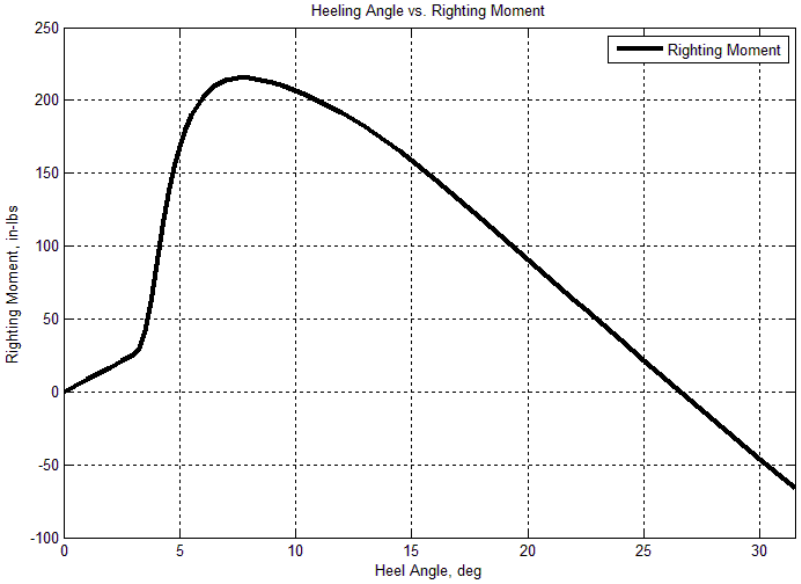

Figure 31. Righting moment vs. Heel angle for baseline SSF.

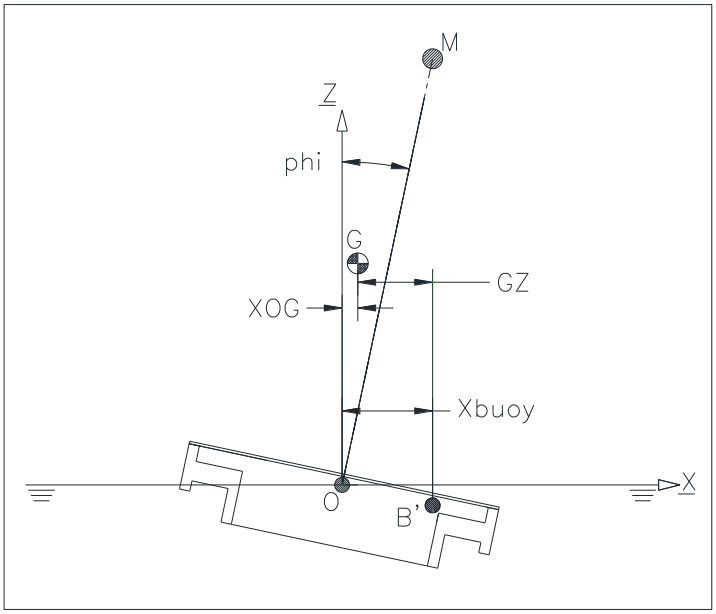

Figure 32. Righting lever diagram.

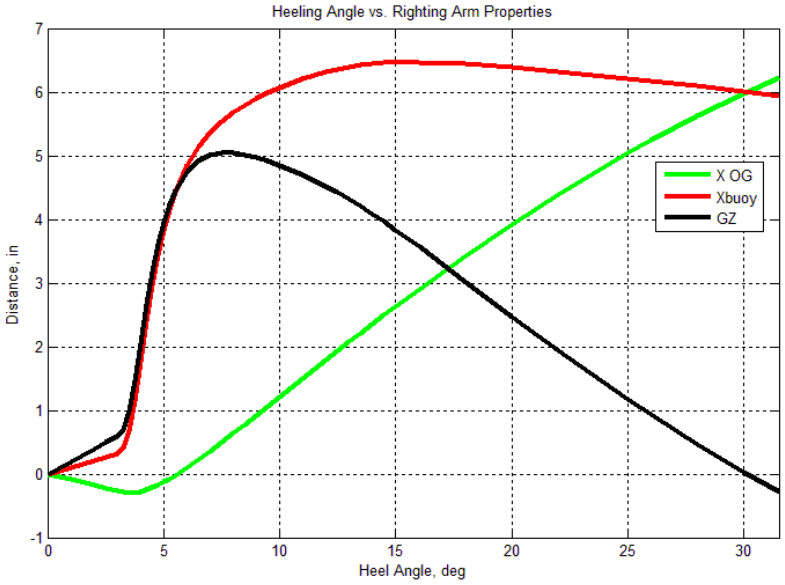

Figure 33. Righting lever vs. Heel angle for baseline SSF.

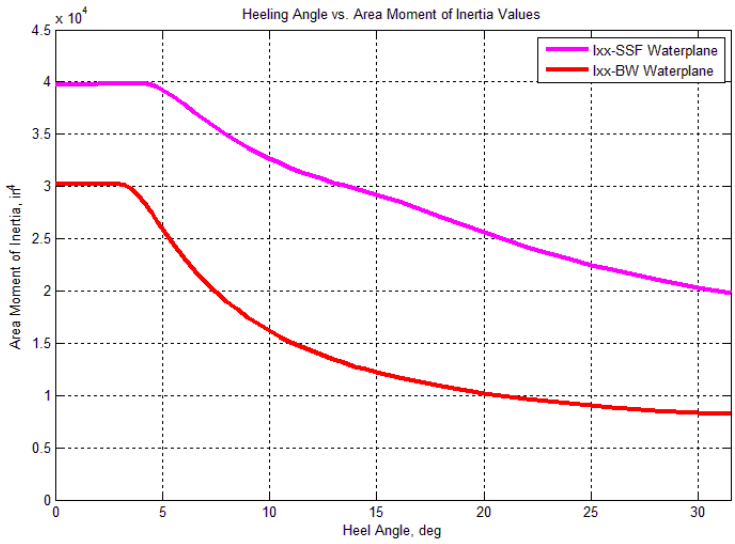

Figure 34. Water plane moment of inertia vs. Heel angle

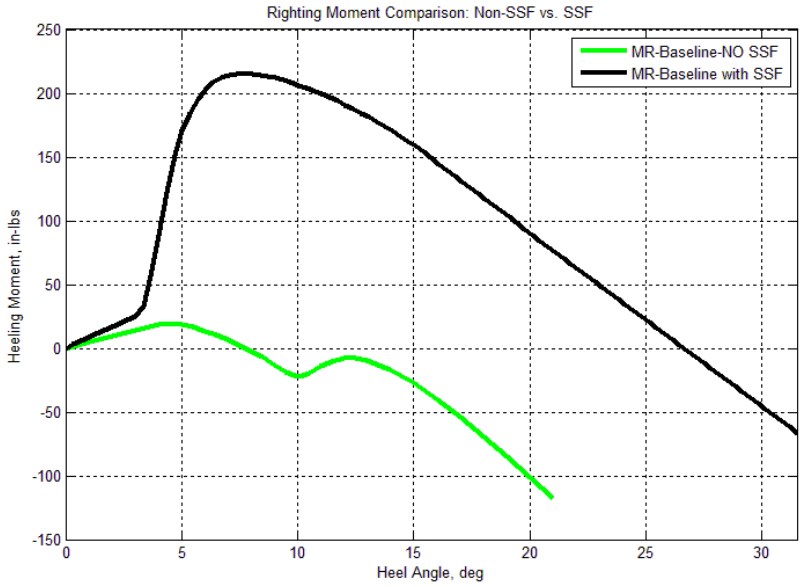

Figure 35. Comparison of non-SSF and SSF righting moment.

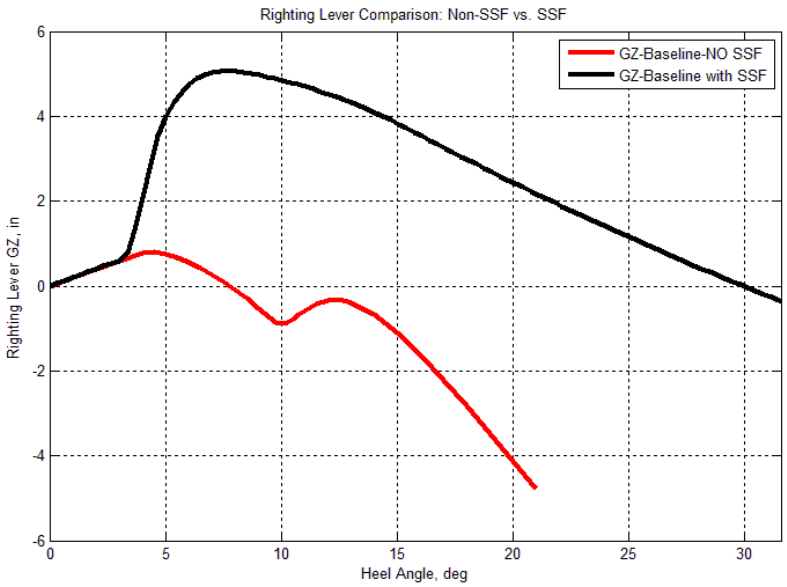

Figure 36. Comparison of non-SSF and SSF righting lever.

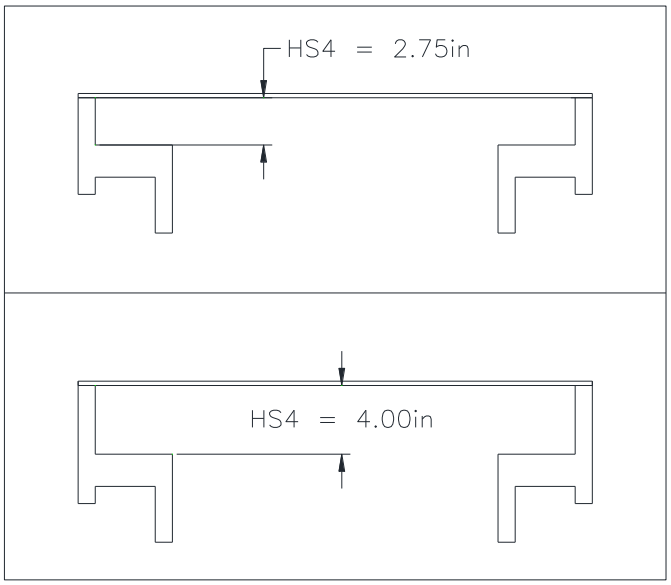

Figure 37. Section 4 height variations.

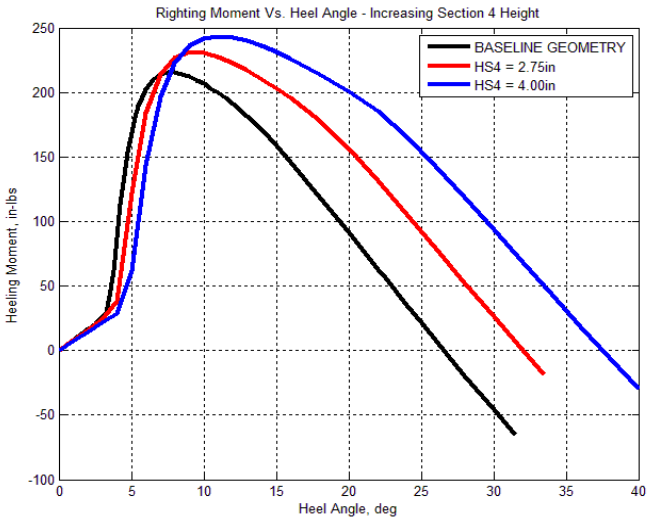

Figure 38. Righting moment vs. Heel angle for varying Section 4 heights.

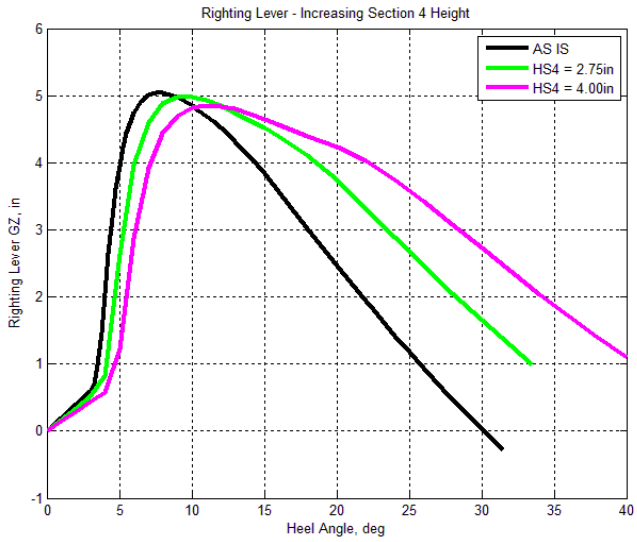

Figure 39. Righting lever vs. Heel angle for varying Section 4 heights.

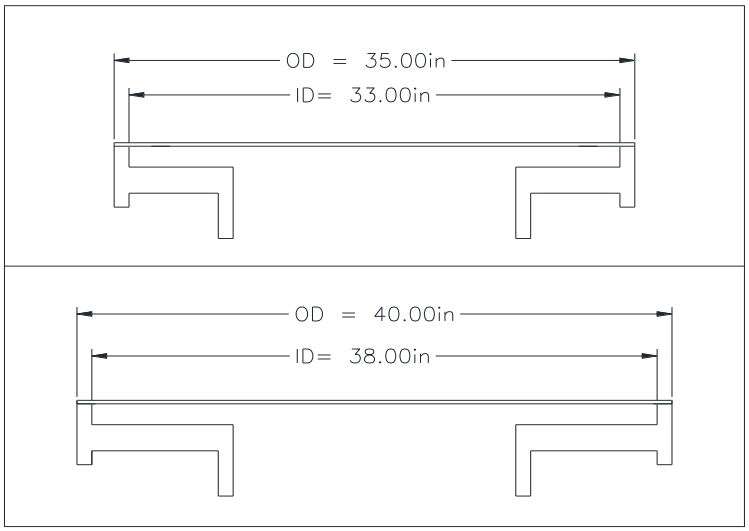

Figure 40. Section 4 diameter variations.

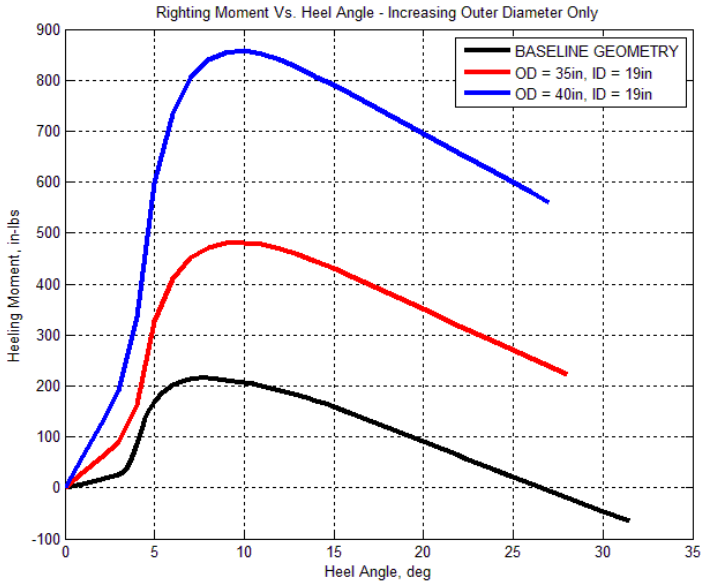

Figure 41. Righting moment vs. Heel angle for varying Section 4 diameters.

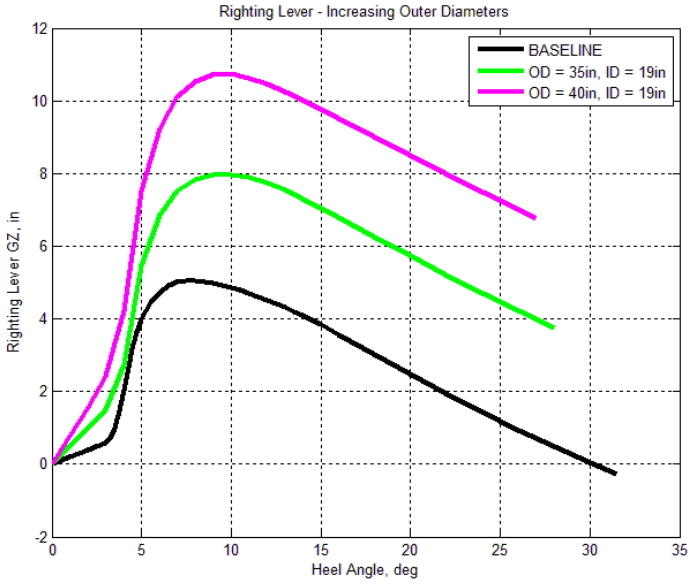

Figure 42. Righting lever vs. Heel angle for varying Section 4 diameters.

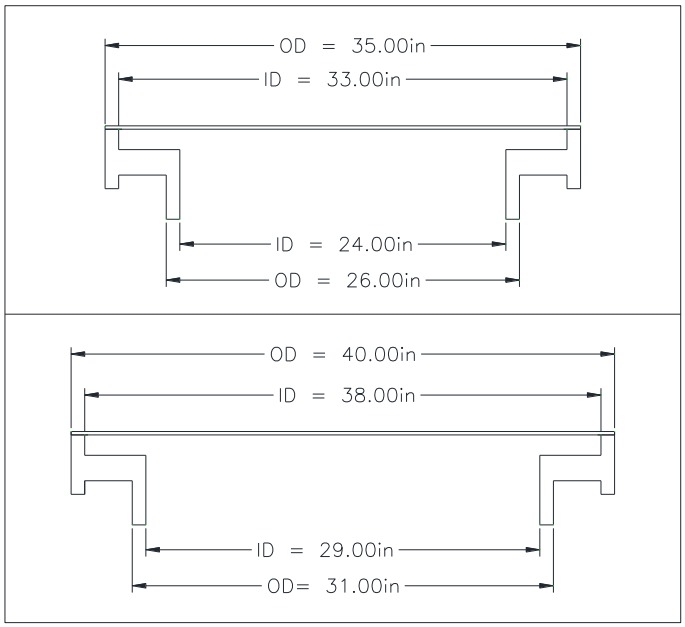

Figure 43. All section diameter variations

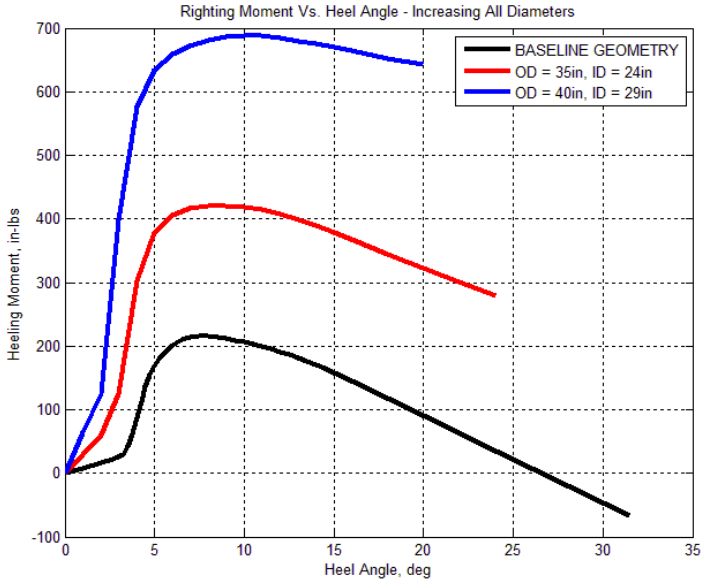

Figure 44. Righting moment vs. Heel angle for varying all section diameters.

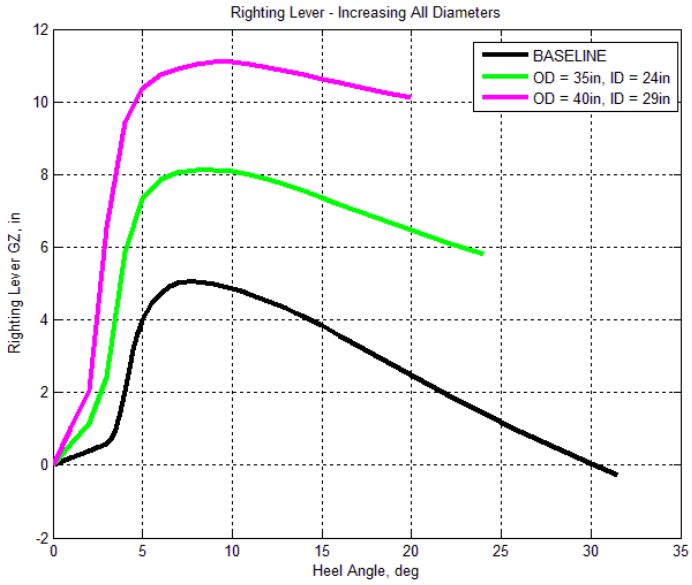

Figure 45. Righting lever vs. Heel angle for varying all section diameters.

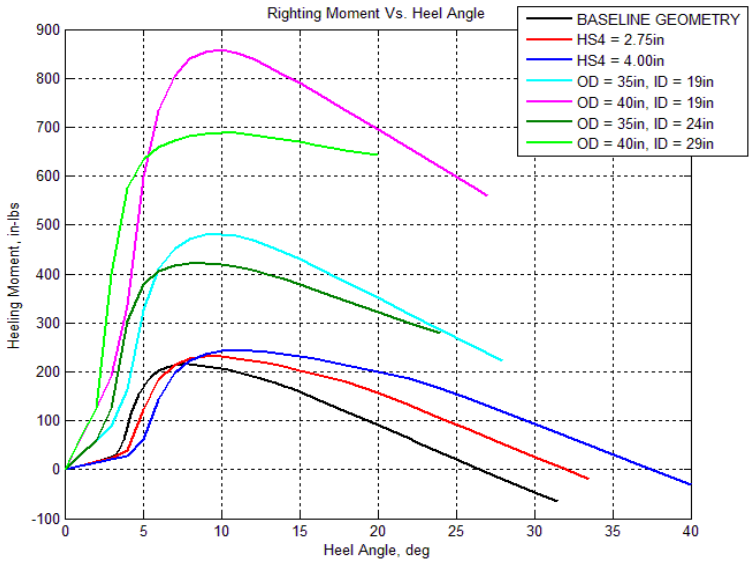

Figure 46. Righting moment vs. Heel angle for all geometric variations.

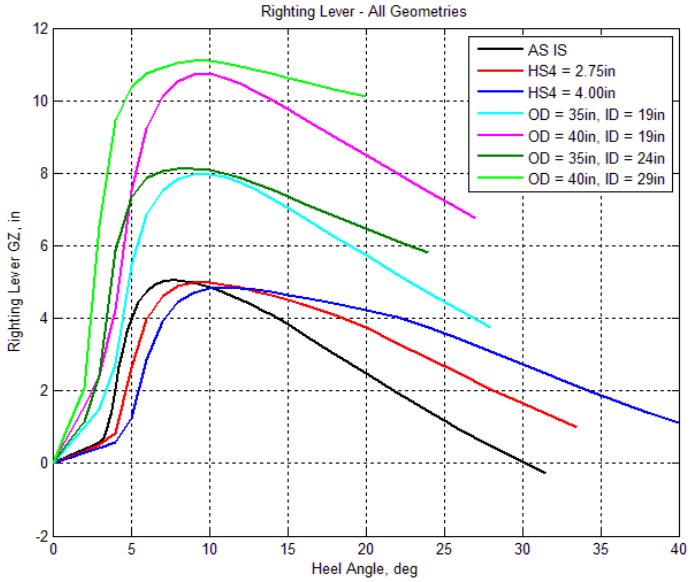

Figure 47. Righting lever vs. Heel angle for all geometric variations.



Figure 48. Experimental SSF



Figure 49. Actual draught of experimental SSF.

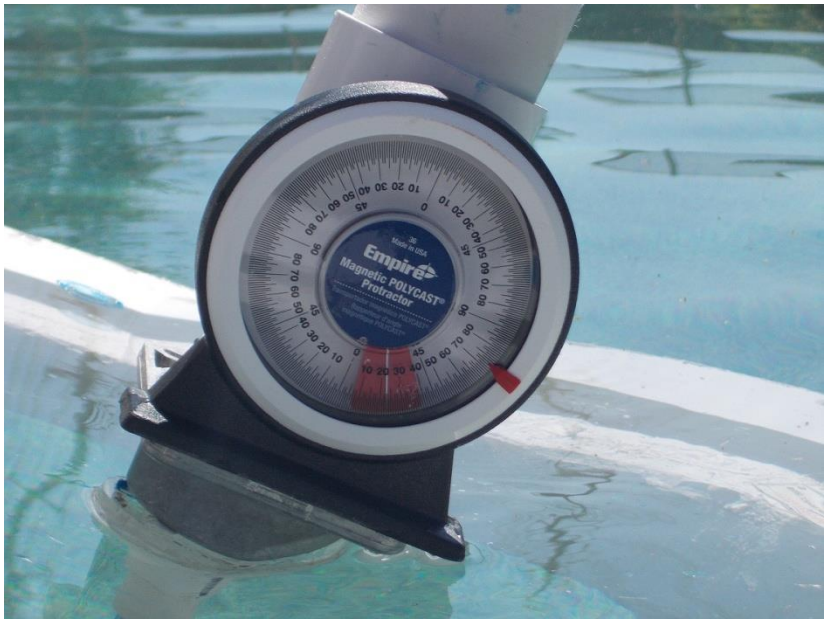

Figure 50. Heeled experimental SSF

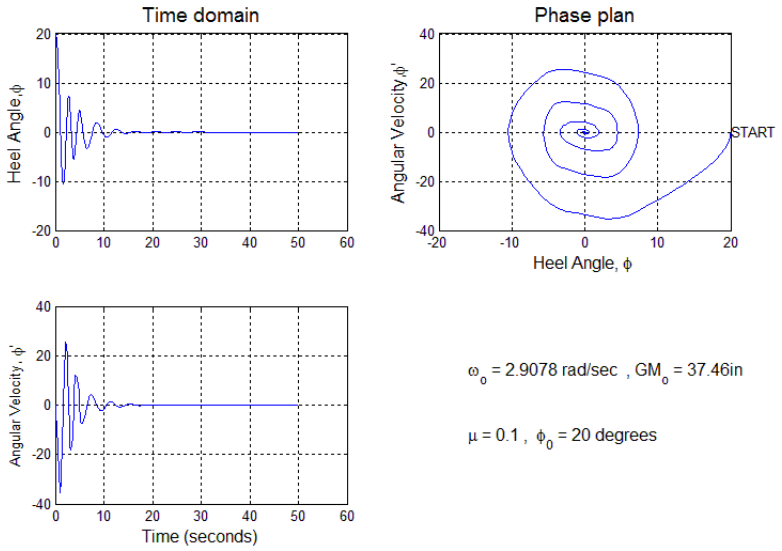

Figure 51. Roll amplitude for baseline SSF heeled to 22 degree

Table Caption List

Table 1 Density of SSF and submerging fluid.

Table 2 Section properties of baseline SSF

Table 3 Mass properties of baseline SSF

Table 4 Comparison of non-SSF and SSF

Table 5 Mast properties

Table 6 Range of mast weights for comfortable float motion

Table 7 Hydrostatic properties of SSF with mast

Table 8 Comparison of hydrostatic properties of non-SSF and SSF

Table 9 Geometric properties by varying section 4 height

Table 10 Geometric properties after varying section 4 diameters

Table 11 Geometric properties by varying all section diameters

Table 12 Maximum righting moment values

Table 13 Maximum righting lever values

Table 14 Angles of vanishing stability and air entrance angles

Table 15 Calculated properties for experimental SSF

Table 16 Comparison of all geometric variations

Table 1. Density of SSF and submerging fluid.

Density of Salt Water	0.0370 lbs/in^3
Density of SSF Body	0.0017 lbs/in^3
Density of SSF Top Plate	0.0425 lbs/in^3

Table 2. Section properties of baseline SSF

	Height (in)	Ab(in^2)	Aw(in^2)	Vb (in^3)	Vw (in^3)	Vtot (in^3)	Ib (in^3)	Iw (in^3)	Itot (in^3)
Section 1	2.250	62.800	283.500	141.30	637.88	779.18	3,149.00	6,398.00	9,547.00
Section 2	1.000	154.000	552.900	154.00	552.90	706.90	12,738.00	27,024.00	39,762.00
Section 3	1.875	423.300	283.500	793.69	531.56	1,325.25	33,364.00	6,348.00	39,762.00
Section 4	1.500	91.100	615.800	136.65	923.70	1,060.35	9,589.00	30,172.00	39,762.00
Section 5	0.250	706.900	N/A	176.73	N/A	176.73	39,762.00	N/A	39,762.00
TOTAL	6.875	N/A	N/A	1402.363	2646.038	4048.400	N/A	N/A	N/A

Table 3. Mass properties of baseline SSF

	mb (lbf)	mw (lbf)	mtot (lbf)
Section 1	0.240	23.601	23.842
Section 2	0.262	20.457	20.719
Section 3	1.349	19.668	21.017
Section 4	0.232	34.177	34.409
Section 5	7.511	N/A	7.511
TOTAL	9.594	97.903	107.498

Table 4. Comparison of non-SSF and SSF

	Baseline SSF		Baseline Without SSF	
Total Weight	40.74	lbf	9.59	lbf
Draught, in	5.26	in	3.02	in
Displacement Volume	1101.90	in^3	259.30	in^3
KB, in	3.69	in	1.81	in
KG, in	5.98	in	6.12	in
BM, in	36.11	in	49.13	in
GM, in	33.73	in	44.82	in
If , in	27.40	in	N/A	
GMeff, in	61.13	in	N/A	

Table 5. Mast properties

Mast Height, in	Mast Cylinder KG, in	Concentrated Mass KG, in	Total KG, in
15.00	14.38	21.88	16.63
30.00	21.88	36.88	26.63
45.00	29.38	51.88	36.63
60.00	36.88	66.88	46.63
75.00	44.38	81.88	56.63
90.00	51.88	96.88	66.63
105.00	59.38	111.88	76.63

Table 6. Range of mast weights for comfortable float motion

Mast Height, in	Weight when Kempf's Factor = 8, lbf	Weight when Kempf's Factor = 14, lbf
15.00	N/A	N/A
30.00	N/A	N/A
45.00	N/A	N/A
60.00	N/A	N/A
75.00	28.30	N/A
90.00	22.40	33.00
105.00	17.80	27.00

Table 7. Hydrostatic properties of SSF with mast

	Baseline
Mast Weight	15.00 lbf
Mast Height	92.00 in
Mast KG	65.00 in
Ballast Water Weight	18.08 lbf
Ballast Water Volume	488.70 in^3
Ballast Water KG	6.23 in
Total Weight	42.68 lbf
Draught, in	5.83 in
Displacement Volume	1153.40 in^3
KB, in	3.69 in
KG, in	26.86 in
BM, in	34.47 in
GM, in	11.30 in
lf , in	26.16 in
GMeff, in	37.46 in

Table 8. Comparison of hydrostatic properties of non-SSF and SSF

	Baseline SSF	Baseline Without SSF
Total Weight	42.68 lbf	24.59 lbf
Draught, in	5.83 in	4.12 in
Displacement Volume	1153.40 in^3	664.70 in^3
KB, in	3.69 in	2.93 in
KG, in	26.86 in	42.03 in
BM, in	34.47 in	50.19 in
GM, in	11.30 in	11.09 in
lf , in	26.16 in	N/A
GMeff, in	37.46 in	N/A

Table 9. Geometric properties by varying section 4 height

	Baseline	Height S4 = 2.75in	Height S4 = 4.00in
Mast Weight	15.00 lbf	15.00 lbf	15.00 lbf
Mast Height	92.00 in	92.00 in	92.00 in
Mast KG	65.00 in	65.00 in	65.00 in
Ballast Water Weight	18.08 lbf	21.58 lbf	25.09 lbf
Ballast Water Volume	488.70 in^3	583.35 in^3	677.99 in^3
Ballast Water KG	6.23 in	7.40 in	8.58 in
Total Weight	42.68 lbf	46.37 lbf	50.07 lbf
Draught, in	5.83 in	6.926 in	8.024 in
Displacement Volume	1153.40 in^3	1253.30 in^3	1353.20 in^3
KB, in	3.69 in	3.91 in	4.17 in
KG, in	26.86 in	25.97 in	25.38 in
BM, in	34.47 in	31.73 in	29.38 in
GM, in	11.30 in	9.66 in	8.18 in
lf , in	26.16 in	27.07 in	22.30 in
GMeff, in	37.46 in	33.74 in	30.47 in
Kempf's Factor	7.75	7.86	7.98

Table 10. Geometric properties after varying section 4 diameters

	Baseline	OD = 35in, ID = 19in	OD = 40in, ID = 19in
Mast Weight	15.00 lbf	15.00 lbf	15.00 lbf
Mast Height	92.00 in	92.00 in	92.00 in
Mast KG	65.00 in	65.00 in	65.00 in
Ballast Water Weight	18.08 lbf	32.30 lbf	48.81 lbf
Ballast Water Volume	488.70 in^3	872.79 in^3	1319.00 in^3
Ballast Water KG	6.23 in	6.12 in	6.04 in
Total Weight	42.68 lbf	60.48 lbf	81.13 lbf
Draught, in	5.83 in	5.605 in	5.462 in
Displacement Volume	1153.40 in^3	1634.60 in^3	2192.60 in^3
KB, in	3.69 in	3.81 in	3.89 in
KG, in	26.86 in	20.72 in	16.96 in
BM, in	34.47 in	45.07 in	57.31 in
GM, in	11.30 in	28.15 in	44.24 in
If , in	26.16 in	35.61 in	46.68 in
GMeff, in	37.46 in	63.77 in	90.92 in
Kempf's Factor	7.75	4.69	3.23

Table 11. Geometric properties by varying all section diameters

	Baseline	OD = 35in, ID = 24in	OD = 40in, ID = 29in
Mast Weight	15.00 lbf	15.00 lbf	15.00 lbf
Mast Height	92.00 in	92.00 in	92.00 in
Mast KG	65.00 in	65.00 in	65.00 in
Ballast Water Weight	18.08 lbf	23.96 lbf	29.54 lbf
Ballast Water Volume	488.70 in^3	647.55 in^3	798.32 in^3
Ballast Water KG	6.23 in	6.25 in	6.27 in
Total Weight	42.68 lbf	51.70 lbf	60.83 lbf
Draught, in	5.83 in	5.868 in	5.921 in
Displacement Volume	1153.40 in^3	1397.20 in^3	1644.10 in^3
KB, in	3.69 in	3.68 in	3.68 in
KG, in	26.86 in	23.28 in	20.74 in
BM, in	34.47 in	55.72 in	76.43 in
GM, in	11.30 in	33.13 in	59.38 in
If , in	26.16 in	41.67 in	62.26 in
GMeff, in	37.46 in	74.80 in	121.63 in
Kempf's Factor	7.75	4.65	3.18

Table 12. Maximum righting moment values

	Heel Angle (Deg)	Maximum Righting Moment (in-lbs)
Baseline	8	215.3
HS4 = 2.75in	10	231.32
HS4 = 4.00in	12	243.52
OD = 35in, ID = 24in	10	420.64
OD = 35in, ID = 19in	11	481.26
OD = 40in, ID = 29in	11	689.02
OD = 40in, ID = 19in	11	857.58

Table 13. Maximum righting lever values

	Heel Angle (Deg)	Maximum Righting Lever (in)
HS4 = 4.00in	12	4.849
HS4 = 2.75in	10	4.984
Baseline	8	5.044
OD = 35in, ID = 19in	11	7.9711
OD = 35in, ID = 24in	10	8.111
OD = 40in, ID = 19in	11	10.735
OD = 40in, ID = 29in	11	11.087

Table 14. Angles of vanishing stability and air entrance angles

	Angle of Vanishing Stability (deg)	Air Entrance Angle (deg)
Baseline	26.5	31.5
HS4 = 2.75in	32	33.5
HS4 = 4.00in	37	40
OD = 35in, ID = 19in	N/A	28
OD = 40in, ID = 19in	N/A	27
OD = 35in, ID = 24in	N/A	24
OD = 40in, ID = 29in	N/A	20

Table 15. Calculated properties for experimental SSF

	Experimental
Mast Weight	9.50 lbf
Mast KG	65.00 in
Ballast Water Weight	21.91 lbf
Ballast Water Volume	606.98 in^3
Ballast Water KG	6.13 in
Total Weight	41.01 lbf
Draught, in	5.63 in
Displacement Volume	1135.90 in^3
KB, in	3.66 in
KG, in	19.77 in
BM, in	35.01 in
GM, in	18.90 in
lf , in	26.56 in
GMeff, in	45.46 in
Kempf's Factor	5.77

Table 16. Comparison of all geometric variations

	No Suction Stabilization	Section 4 Height	Section 4 Diameter	All Section Diameters
Metacentric Height	(-)	(-)	**(+)**	**(+)**
Roll Period	**(+)**	**(+)**	(-)	(-)
Kempf Factor	**(+)**	**(+)**	(-)	(-)
Angle of Vanishing Stability	(-)	**(+)**	**(+)**	**(+)**
Air Entrance Angle	(-)	**(+)**	(-)	(-)
Righting Moment	(-)	**(+)**	**(+)**	**(+)**
Righting Lever	(-)	(-)	**(+)**	**(+)**

(+) - Indicates an Increase from the Baseline SSF
(-) - Indicates an Increase from the Baseline SSF